INTERNATIONAL ATOMIC ENERGY AGENCY
UNITED NATIONS EDUCATIONAL, SCIENTIFIC AND CULTURAL ORGANIZATION
INTERNATIONAL CENTRE FOR THEORETICAL PHYSICS
I.C.T.P., P.O. BOX 586, 34100 TRIESTE, ITALY, CABLE CENTRATOM TRIESTE

H4.SMR/453-36

TRAINING COLLEGE ON PHYSICS AND CHARACTERIZATION OF LASERS AND OPTICAL FIBRES

(5 February - 2 March 1990)

PULSE COMPRESSION IN SINGLE-MODE FIBERS - PICOSECONDS TO FEMTOSECONDS

A.M. Johnson
&
C.V. Shank

AT & T Bell Laboratories
Holmdel, U.S.A.

Matveętz, Yu. A., S.V. Chekalin, and A.V. Sharkov (1985) J. Opt. Soc. Am. B 2, 634.
Menyuk, N. and D.K. Killinger (1983) Appl. Opt. 22, 2690.
Monger, T.G., R.R. Alfano, and R.H. Callender (1979) Biophys. J. 27, 105.
Moore, D.S. and S.C. Schmidt (1987) Opt. Lett. 12, 480.
Owens, J.C. (1967) Appl. Opt. 6, 51; and Topp, M. and G. Orner (1975) Opt. Commun. 13, 276.
Palfrey, S.L. and D. Grischkowsky (1985) Opt. Lett. 10, 562.
Rothberg, L., T.M. Jedju, S. Etemad, and G.L. Baker (1986) Phys Rev. Lett. 57, 3229.
Saha, S.K. and R.W. Hellwarth (1983) Phys. Rev. A 27, 919.
Saux, G. Le, F. Salin, P. Georges, G. Roger, and A. Brun (1988) Appl. Opt. 27, 777.
Schoenlein, R.W., W.Z. Lin, J.G. Fujimoto, and G.L. Eesley (1986) In *Ultrafast Phenomena V*, G.R. Fleming and A.E. Siegman, eds., p. 260. Springer-Verlag, New York.
Shank, C.V., R.L. Fork, R.T. Yen, R.J. Stolen, and W.J. Tomlinson (1982) Appl. Phys. Lett. 40, 761.
Searle, G.F.W., J. Barbet, G. Porter, and C.J. Tredwell (1978) Biochim. Biophys. Acta 501, 246 256.
Singer, S.S. (1969) Appl. Opt. 7, 1125.
Thomas, D.G., L.K. Anderson, M.I. Cohen, E.I. Gordon, and P.K. Runge (1982) In *Innovations in Telecommunications*, J.T. Manassah, ed., Academic Press, New York.
Tomlinson, W.J., R.H. Stolen, and C.V. Shank (1984) J. Opt. Soc. Am. B 1, 139.
Treacy, E.B. (1969) IEEE J. Quantum Electron. QE-5, 454.
Tsuchiya, Y. (1983) "Picosecond streak camera and its applications," Hamamatsu Tech. Bull. 14, June; C.S. Gardner, B.M. Tsai, and K.F. Im (1983) Appl. Opt. 22, 2571; Abshire, J.B. and G.E. Kalshoven (1983) Appl. Opt. 22, 2578.
Valdmanis, J.A. (1986) In *Ultrafast Phenomena V*, Fleming and Siegman, eds., p. 82.
von der Linde, D., and R. Lambrich (1979) Phys. Lett. 42, 1090.
Williams, R.T., B.B. Craig, and W.L. Faust (1984) Phys. Rev. Lett. 52, 1709.
Wong, D. (1982) In *Biological Events Probed by Ultrafast Laser Spectroscopy*, R.R. Alfano, ed., chapter 1. Academic Press, New York.
Zysset, B., W. Hodel, P. Beaud, and H.P. Weber (1986) Opt. Lett. 11, 156.

10
Pulse Compression in Single-Mode Fibers—Picoseconds to Femtoseconds

A.M. JOHNSON and C.V. SHANK

1. Introduction

The compression of frequency swept (in time) or "chirped" optical pulses was independently proposed by Gires and Tournois (1964) and Giordmaine et al. (1968). Optical pulse compression is the optical analog of microwave pulse compression or chirp radar developed by Klauder et al. (1960). The compression is accomplished in two steps. First, an optical frequency sweep is impressed on the pulse. The next step is the compensation of this frequency sweep by using a dispersive delay line, where the group velocity or group delay varies with optical frequency. Ideally, the dispersive delay line would impress the opposite chirp on the pulse, resulting in the compression of the pulse to its minimum width, $\sim 1/\Delta\omega$, where $\Delta\omega$ is the frequency sweep. Treacy (1968, 1969) was the first to recognize that a pair of diffraction gratings was a suitable dispersive delay line for a linearly chirped pulse; he used gratings to compress the inherently chirped output of a mode-locked Nd:glass laser. Similar experiments were later performed by Bradley et al. (1970). Duguay and Hansen (1969) used an $LiNbO_3$ phase modulator and Gire-Tournois interferometer to compress pulses from a mode-locked He-Ne laser.

A chirp can be impressed on a intense optical pulse as it passes through a medium with an intensity-dependent refractive index, i.e., an optical Kerr medium. The phase of the intense optical pulse is modulated by the nonlinear refractive index. Extreme small spectral broadening of optical pulses in optical Kerr liquids was first observed in self-focused filaments by Bloembergen and Lallemand (1966), Brewer (1967), and Ueda and Shimoda (1967). The weak spectral broadening was first explained by Shimizu (1967) as due to a rapid time-varying phase shift arising from the nonlinear refractive index. Gustafson et al. (1969) further elaborated on Shimizu's explanation with detailed numerical calculations of the spectra of self-phase-modulated pulses, including the effects of dispersion and relaxation of the nonlinearity. Alfano and Shapiro (1970) made the first measurements of self-phase modulation (SPM) in crystals, liquids, and glasses (see Chapter 2). Spectral broadening data in glasses were also obtained by Bondarenko et al. (1970).

Fisher et al. (1969) suggested that optical pulses in the range 10^{-13} to 10^{-14} s could be achieved as a result of the SPM obtained by passing a short pulse through an optical Kerr liquid followed by a dispersive delay line. Laubereau (1969) used several cells of the optical Kerr liquid CS_2 and a pair of diffraction gratings to compress 20-ps-duration pulses from a mode-locked Nd:glass laser by 10×. Zel'dovich and Sobel'man (1971) proposed the possibility of using alkali metal vapors to both spectrally broaden optical pulses by SPM and compress the pulses by the strong dispersion of the group velocity near the atomic resonance. Lehmberg and McMahon (1976) compressed 100-ps-duration pulses from a mode-locked and amplified Nd:YAG laser by 14×, using a series of liquid CS_2 cells and diffraction gratings separated by 23 m. Spectral broadening of picosecond pulses from a flashlamp-pumped, passively mode-locked Rhodamine 6G dye laser was reported by Arthurs et al. (1971) and was attributed to SPM. Ippen and Shank (1975b) compressed 1-ps-duration pulses from a CW pumped, passively mode-locked Rhodamine 6G dye laser by 3× to a duration of 0.3 ps using diffraction gratings separated by 10 cm.

The early measurements of SPM (Bloembergen and Lallemand, 1966); Brewer, 1967; Ueda and Shimoda, 1967; Shimizu, 1967; Gustafson et al., 1969; Alfano and Shapiro, 1970; Bondarenko et al., 1970) occurred in self-focused filaments, where the intensity was high and there were problems with competing nonlinear effects and uncertainties concerning the filament size (see Chapter 2). Ippen et al. (1974) reported the first measurement of SPM in the absence of self-trapping or self-focusing with the use of a guiding multimode optical fiber filled with liquid CS_2. Stolen and Lin (1978) reported measurements of SPM is single-mode silica core fibers. In fibers, any additional confinement caused by self-focusing is negligible. An additional advantage of this guiding structure over bulk crystals or liquid cells is that the modulation can be imposed over the entire transverse spatial extent of the beam, and the problem of unmodulated light in the wings of the beam is eliminated (Ippen et al., 1974). Perhaps the most important feature of SPM in optical fibers is that significant spectral broadening can be achieved at power levels much lower than those required in bulk media.

The first fiber pulse compression experiments utilized the fiber as a dispersive delay line to compress chirped optical pulses. Suzuki and Fukumoto (1976) used an $LiNbO_3$ phase modulator to chirp 1-μm laser pulses, which were subsequently compressed by the normal or positive group velocity dispersion (GVD) (red frequencies lead blue) of a silica optical fiber. Wright and Nelson (1977) compressed the chirped output of a GaAs semiconductor laser operating at 0.894 μm using a positive GVD optical fiber delay line. Iwashita et al. (1982) demonstrated 5× compression of 1.7-ns, 1.54-μm pulses from a chirped InGaAsP injection laser using a 104-km negative GVD fiber delay line. Mollenauer et al. (1980) performed the first pulse compression experiments using optical fibers as a Kerr medium, in their work on soliton compression of pulses from a color center laser. In these experiments the laser

wavelength (λ = 1.55 μm) was in the anomalous or negative GVD (blue frequencies lead red) region for silica and did not require a separate dispersive delay line. In this instance, the fiber material forms an integrated dispersive delay line and self-compresses the pulse. Using soliton compression, Mollenauer et al. (1983) compressed 7-ps-duration pulses by 27× to a duration of 0.26 ps with a 100-m length of single-mode fiber. This compression was achieved with only 200 W of peak power at the fiber input, thus further attesting the low power requirements of nonlinear effects in optical fibers. It is beyond the scope of this chapter to consider soliton compression in optical fibers. Further information on soliton compression and its applications can be found, for example, in excellent discussions by Mollenauer and co-workers (Mollenauer and Stolen, 1982; Mollenauer, 1985; Mollenauer et al., 1986). This chapter is limited to pulse compression, in silica core fibers, in the normal or positive GVD region ($\lambda \leq 1.3$ μm), where a separate dispersive delay line is necessary. The compression of positively chirped optical pulses passing through a dispersive medium possessing negative GVD is schematically illustrated in Figure 10.1.

Nakatsuka and Grischkowsky (1981) demonstrated distortion-free pulse propagation of synchronously mode-locked dye laser pulses by using the positive GVD of fibers to chirp the pulses. In this experiment, low-power (to avoid SPM) 3.3-ps dye laser pulses were chirped and temporally broadened to 13 ps and recompressed back to 3.3 ps by the negative GVD of a near-resonant atomic Na-vapor delay line. Subsequently, Nakatsuka et al. (1981) performed the first pulse compression experiment using fibers as a Kerr medium in the positive GVD region. This experiment utilized both the positive

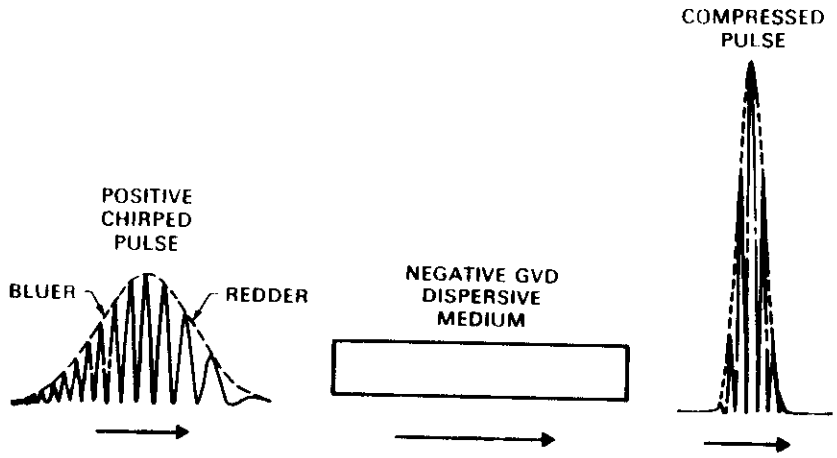

FIGURE 10.1. Compression of positively chirped optical pulses (red frequencies leading blue) using a dispersive medium possessing negative group velocity dispersion (GVD).

GVD and SPM to temporally and spectrally broaden 5.5-ps dye laser pulses with subsequent compression by $>3\times$ to 1.5 ps by passage through a near-resonant atomic Na-vapor delay link. Shank et al. (1982) replaced the atomic vapor delay line with a Treacy (1968; 1969) grating pair to compress the 90-fs amplified output of a colliding-pulse mode-locked (CPM) dye laser by $3\times$ to a duration of 30 fs, using a 15-cm fiber. Subsequently, Nikolaus and Grischkowsky (1983a) compressed the 5.4-ps output of a synchronously mode-locked and cavity-dumped dye laser by $12\times$ to a duration of 450 fs, using a grating-based dispersive delay line and a 30-m fiber. Using two stages of fiber-grating compression, Nikolaus and Grischkowsky (1983b) compressed 5.9-ps pulses from the aforementioned dye laser by $65\times$ to a duration of 90 fs. In the technological push to generate optical pulses of less than 10-fs duration, amplified CPM dye laser pulses were next compressed to 16 fs by Fujimoto et al. (1984). Compression to 12 fs by Halbout and Grischkowsky (1984) was soon followed by compression to 8 fs by Knox et al. (1985). Each of these compression achievements occurred with an important concomitant increase in repetition rate. Recently, Fork et al. (1987) achieved compression to 6 fs, the shortest to date, by using a grating pair followed by a prism sequence in order to compensate the cubic phase distortion of these large-bandwidth pulses by the grating pair.

Optical fiber compression of "long" duration picosecond pulses from CW mode-locked (CWML) Nd:YAG-based systems has also been achieved. Subpicosecond pulses can be generated with these sources without the use of a mode-locked dye laser. In addition, compressed CWML Nd:YAG-based systems can be used as pump sources for synchronously mode-locked dye lasers. Johnson et al. (1984a, 1984b) performed the first "long" pulse fiber compression experiments in a system other than a dye laser. In these experiments, 33-ps pulses at 0.532 μm from a CWML and frequency-doubled Nd:YAG laser were compressed $80\times$ to a duration of 410 fs, using a 105-m fiber and a grating pair. Shortly thereafter, Dianov et al. (1984a) compressed 60-ps pulses, at 1.064 μm from a CWML and Q-switched Nd:YAG laser (1 kHz repetition rate), by $15\times$ to a duration of 4 ps using a 10-m fiber and a grating-based delay line. The compression of 1.064-μm pulses from a CWML Nd:YAG laser was later performed independently by Kafka et al. (1984) and Heritage et al. (1984). Kafka et al. (1984) demonstrated the compression of 80-ps pulses by $45\times$ to a duration of 1.8 ps, while Heritage et al. (1984) compressed 90-ps pulses by $30\times$ to a duration of 3 ps. Dupuy and Bado (1984) reported the compression of 110-ps pulses from a CWML argon-ion laser by $5\times$. Further studies of the compression of 1.064-μm pulses from CWML Nd:YAG lasers were reported by Heritage et al. (1985a), Kafka and Baer (1985), and Gomes et al. (1985a). Using two stages of fiber-grating compression, Gomes et al. (1985b) compressed 85-ps pulses, at 1.064 μm, from a CWML Nd:YAG laser by $113\times$ to a duration of 750 fs. Damm et al. (1985) reported on the use of large-core (50 μm) graded-index fiber to compress 5-ps pulses at 1.054 μm from a mode-locked Nd:phosphate glass laser by $7\times$ to a duration of 700 fs. CWML and Q-switched Nd:YAG laser pulses at 1.064 μm were compressed $29\times$ to a duration of 2.9 ps by Gomes et al. (1985c) in a manner similar to that reported by Dianov et al. (1984). Blow et al. (1985) reported on all-fiber compression of a CWML Nd:YAG laser at 1.32 μm by adjusting the waveguide dispersion of two lengths of fiber. In this experiment, 130-ps pulses were compressed to a photodiode limit of 70 ps by using a dispersion-shifted positive GVD fiber followed by a negative GVD fiber. Kai and Tomita (1986a) reported the compression of 100-ps pulses at 1.32 μm from a CWML Nd:YAG laser by $50\times$ to a duration of 2 ps using 2 km of dispersion-shifted fiber and a grating pair. Using two stages of fiber-grating compression, Zysset et al. (1986) compressed 90-ps pulses, at 1.064 μm, from a CWML Nd:YAG laser by $450\times$ to a duration of 200 fs. Kai and Tomita (1986b) demonstrated the compression of 100-ps, 1.32-μm pulses from a CWML Nd:YAG laser by $1100\times$ to a duration of 90 fs by using one stage of fiber-grating compression (dispersion-shifted fiber) followed by soliton compression in a length of negative GVD fiber.

In Section 2 we present results for picosecond fiber-grating compression in a normalized form, from which one can calculate the optimum fiber length, the achievable compression, and the proper grating separation for a given input pulse and fiber. Section 3 deals with the subtleties and nuances of femtosecond fiber pulse compression, that is, higher order dispersion compensation of very large bandwidth pulses.

2. Picosecond Pulse Compression

2.1 Optical Kerr Medium

Optical fibers are usually considered to be linear media; that is, as the input power is increased, one expects only a proportional increase in output power (Stolen, 1979b). However, dramatic nonlinear effects can occur that can cause strong frequency conversion, optical gain, and many other effects generally associated with very intense optical pulses and highly nonlinear optical materials. These nonlinear processes depend on the interaction length as well as the optical intensity. In small-core fibers high intensities can be maintained over kilometer lengths. If this length is compared with the focal region of a Gaussian beam of comparable spot size, enhancements of 10^5 to 10^8 are possible using fibers. This enhancement lowers the threshold power for nonlinear processes—in some cases to less than 100 mW (Stolen, 1979b). For example, single-mode fibers with core diameters less than 10 μm possess core areas of $<10^{-6}$ cm^2, which serves to translate powers in watts to intensities of MW/cm^2. An intensity-dependent refractive index leads to SPM and self-focusing within a single optical pulse. In fibers, however, any additional confinement caused by self-focusing is negligible (Stolen and Lin, 1978). Recently, Baldeck et al. (1987) reported on the observation of self-focusing in

optical fibers with 25-ps pulses from an active-passive mode-locked and frequency-doubled Nd:YAG laser. (see Chapter 4) There are several caveats to this observation of self-focusing: (1) self-focussing occurred with pulse energies greater than 10 nJ, in a multimode fiber with a core diameter of 100 μm; (2) self-focusing appeared primarily at Stokes-shifted stimulated Raman frequencies, for which the effectof the nonlinear refractive index is enhanced by cross-phase modulation; (3) self-focusing occurred at stimulated Raman conversion efficiencies of approximately 50%. The experimental conditions under which Baldeck et al. (1987) were able to observe self-focusing lend further substantial support to the claim that self-focusing is negligible under the standard experimental conditions for pulse compression in single-mode fibers. Hence single-mode fibers represent a nearly ideal nonlinear Kerr medium for the generation of the SPM necessary for pulse compression.

Fisher et al. (1969) suggested that picosecond pulses could be compressed to femtosecond durations by employing the large positive chirp obtainable near the center of a short pulse as a result of SPM in optical Kerr liquids. SPM results from the passage of an intense pulse through a medium with an intensity-dependent refractive index. When the relaxation time of the nonlinearity is much less than the input pulse duration, the region where the positive chirp is largest and least dependent on time occurs at about the peak of the pulse and large compression ratios are possible. For longer relaxation times, this region is delayed with respect to the peak of the pulse. Compression is diminished by the influence of relaxation, which not only delays the maximum chirp but also decreases the linear chirp in magnitude and extent. In the limit of the input pulse duration being much shorter than the relaxation time, the resultant chirp would be nonzero only on the wings of the pulse. In fact, if such a pulse were passed through the dispersive delay line, the most intense portion would remain uncompressed. Consequently, Fisher et al. (1969) limited their discussion to picosecond (>5 ps) pulses incident on Kerr liquid CS_2. The dominant contribution to the optical Kerr effect in CS_2 is molecular orientation, with a relaxation time of ~ 2 ps (Shapiro and Broida, 1967; Ippen and Shank, 1975a). In the optical Kerr gate experiments of Ippen and Shank (1975a) utilizing subpicosecond pulses incident on CS_2, the asymmetries in the transmission of the optical gate have been attributed to the relatively long relaxation time. In the case of fused silica, the dominant contribution to the Kerr coefficient is the optically induced distortion of the electronic charge distribution and is expected to have a relaxation time of $\sim 10^{-15}$ s (Alfano and Shapiro, 1970; Owyoung et al., 1972; Duguay, 1976). Thus, relaxation time effects should be negligible, even for the case of femtosecond duration input pulses, for compression in silica fibers.

In general, when an intense optical pulse passes through a nonlinear medium, the refractive index n is modified by the electric field E,

$$n = n_0 + n_2\langle E^2(t)\rangle + \cdots, \tag{1}$$

where n_0 is the refractive index at arbitrarily low intensity and n_2 is the optical

Kerr coefficient (see Chapters 1 and 2). The time-dependent portion of the refractive index modulates the phase of the pulse as it propagates through the medium. A phase change $\delta\phi(t)$ is therefore impressed on the propagating pulse:

$$\delta\phi(t) = n_2\langle E^2(t)\rangle\frac{\omega z}{c}, \tag{2}$$

where ω is the optical frequency, z is the distance traveled in the Kerr medium, and c is the velocity of light. When relaxation time effects can be neglected, according to Shimizu (1967) and DeMartini et al. (1967), the approximate frequency shift at any retarded time (t) is given by the time derivative of the phase perturbation, which is therefore proportional to the time derivative of the pulse intensity

$$\delta\omega(t) = -\frac{d}{dt}\delta\phi(t) = -\frac{\omega z}{c}n_2\frac{d}{dt}\langle E^2(t)\rangle. \tag{3}$$

The instantaneous frequency $\omega(t)$ will shift from the input optical frequency ω_0 by an amount that depends on the intensity profile

$$\omega(t) = \omega_0\left[1 - \frac{z}{c}n_2\frac{d}{dt}\langle E^2(t)\rangle\right]. \tag{4}$$

A positive value of n_2 for silica implies that the increasing intensity in the leading edge of a short pulse results in an increasing refractive index, or a decreasing wave velocity. As a result of the negative sign in Eq. (4), the instantaneous frequency of the leading edge of the pulse will decrease with respect to ω_0. This time-dependent slowing of the wave reduces the rate at which the wave fronts pass a given point in the fiber, thus reducing the optical frequency. The leading edge of the pulse is therefore red-shifted. On the trailing edge of the pulse there is a corresponding frequency increase, or blue shift, resulting in an increase in the spectral bandwidth of the pulse.

For the propagation of low-intensity optical pulses the input and output frequency spectra would be the same (Ippen et al., 1974). As the intensity increases, the transmitted spectrum is broadened and spectral interference maxima and minima appear as the peak phase shift passes through multiples of π. As discussed in the next section, the peaks in the self-phase-modulated spectrum can be washed out or filled in by the presence of GVD.

The spectral broadening of an optical pulse is much easier to treat in the time domain than in the frequency domain (Stolen and Lin, 1978). In the time domain the intensity-dependent refractive index causes a phase shift of the center of the pulse with respect to the wings. A phase modulation introduces sidebands on the frequency spectrum. In the absence of GVD, the shape of the pulse does not change with distance along the fiber and the instantaneous phase depends on the pulse intensity. A phase-modulated or chirped

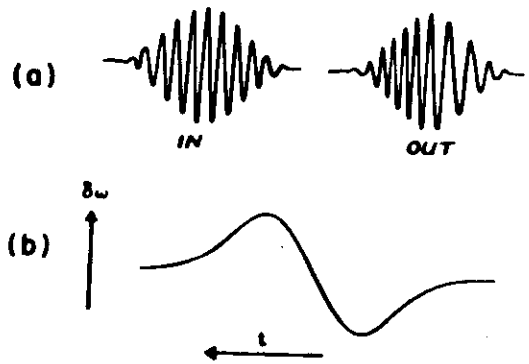

FIGURE 10.2. Effect of an intensity-dependent refractive index on the phase and instantaneous frequency of an optical pulse after propagation down a single-mode fiber.

in the leading half of the pulse and higher, than the carrier frequency, in the trailing half of the pulse. The magnitude of this frequency chirp, in the absence of pulse-shaping effects, builds up in direct proportion to the length of fiber traversed. As illustrated in Figure 10.2b, there is a nearly linear chirp through the central part of the pulse. This region of linear chirp (positive) can be compressed by the linear dispersion (negative) of a grating-pair delay line, by reassembling its frequency components. Treacy (1978, 1979) showed that when two wavelength components, λ and λ' are incident on a grating pair, the longer wavelength experiences a greater group delay. This group delay is determined by the optical path length traversed. With reference to Figure 10.3a, the relationship between the first-order diffraction angles is

$$\sin(\gamma - \theta) = \frac{\lambda}{d} - \sin\gamma$$

where d is the grating ruling spacing, θ is the acute angle between incident and diffracted rays, and γ is the angle of incidence measured with respect to the grating normal. The slant distance AB between the gratings is b, which equals $G \sec(\gamma - \theta)$ where G is defined as the perpendicular distance between the gratings. The ray path length $PABQ$ (see Figure 10.3a) is given by

$$p = b(1 + \cos\theta) = c\tau$$

where τ is the group delay. After considerable algebraic manipulation, the variation of the group delay with wavelength, for various ray path lengths, is found by differentiating p/c with respect to λ leading to

$$\frac{\partial\tau}{\partial\lambda} = \left(\frac{b}{d}\right)\left(\frac{\lambda}{d}\right)\frac{1}{c[1 - (\lambda/d - \sin\gamma)^2]}$$

(see also Chapter 9).

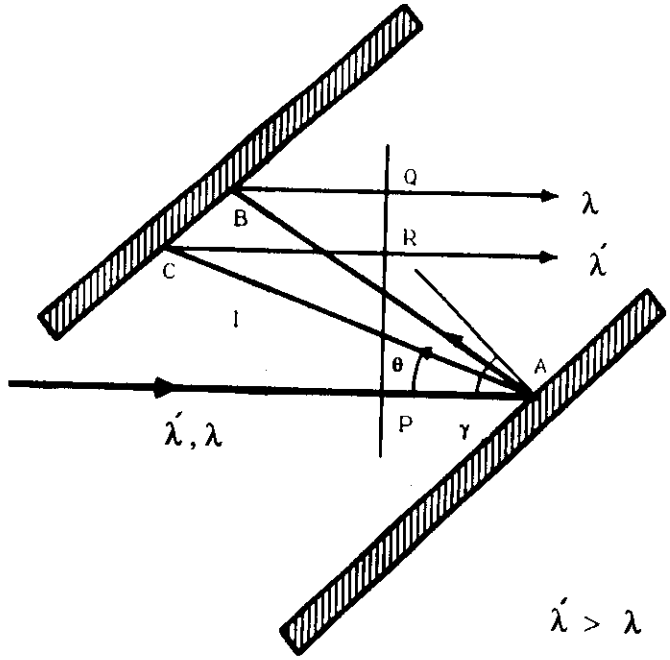

FIGURE 10.3. (a) Treacy (1978, 1979) "single-pass" geometrical arrangement of diffraction gratings used for pulse compression. The angle of incidence with respect to the grating normal is γ, and θ is the acute angle between the incident and diffracted rays. The ray paths are shown for two wavelength components with $\lambda' > \lambda$. Since the path length for λ' is greater than that for λ, longer wavelength components experience a greater group delay. (b) A positively chirped optical pulse with red (R) frequencies leading the blue (B) incident on a typical "double-pass" grating-pair compressor.

A typical "double-pass" (Johnson et al., 1984a, 1984b) grating-pair dispersive delay line is illustrated in Figure 10.3. Here the first grating disperses the beam and the second grating makes the spectral components parallel. The path for the red-shifted light is longer than that for the blue, so if the spacing is chosen correctly all the spectral components will be lined up after the second grating. However, the spectral components will not be together spatially and the output beam looks like an ellipse with red on one side and blue on the other. This is corrected by reflecting the beam back through the grating pair, and hence "double-pass," which puts the spectral components back together and doubles the dispersive delay; that is, the rays (blue and red) undergo double delay or retrace. Johnson et al. (1984a, 1984b) revived the use of the "double-pass" grating-pair delay line, introduced by Desbois et al. (1973) and Agostinelli et al. (1979), for the temporal expansion (picoseconds to nanoseconds) and shaping of mode-locked Nd:glass and Nd:YAG laser pulses. In large-compression-ratio experiments, the double-pass delay line cancels the large transverse displacement of the spatially dispersed spectral components of the output beam evident in Treacy's (1968, 1969) "single-pass" grating-pair delay line. The first compressor application of the double-pass delay line was in the 80 × compression of mode-locked and frequency-doubled Nd:YAG laser pulses by Johnson et al. (1984a, 1984b).

In the next section the parameters necessary for constructing an optical pulse compressor based on a single-mode fiber and grating pair are described.

2.2 Nonlinear Pulse Propagation and Grating Compression

Tomlinson et al. (1984) and Stolen et al. (1984c) have shown, over a fairly broad range of experimental parameters, that the propagation of short, high-intensity pulses in a single-mode fiber can be accurately described by a model that includes only the lowest-order terms in GVD (positive) and SPM. The pulse propagation is modeled by the dimensionless nonlinear wave (Schrödinger) equation:

$$\frac{\partial \mathcal{E}}{\partial(z/z_0)} = -i\frac{\pi}{4}\left[\frac{\partial^2 \mathcal{E}}{\partial(t/t_0)^2} - 2|\mathcal{E}|^2\mathcal{E}\right], \tag{5}$$

where $\mathcal{E}$ is the (complex) amplitude envelope of the pulse. (For a derivation of the nonlinear wave equation see Chapter 3). The time variable t is a retarded time and is defined such that for any distance z along the fiber, the center of the pulse is at $t = 0$, and we assume an input pulse envelope of the form

$$\mathcal{E}(z = 0, t) = A\,\mathrm{sech}(t/t_0). \tag{6}$$

The normalized length z_0 and the peak amplitude A are defined by

$$z_0 = 0.322\frac{\pi^2 c^2 \tau_0^2}{|D(\lambda)|\lambda^2} = 0.322\frac{\pi^2 c\tau_0^2}{|D|\lambda^2} \tag{7}$$

and

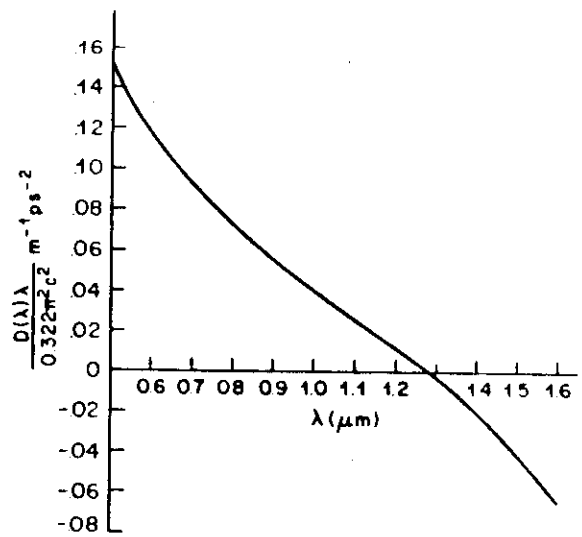

FIGURE 10.4. Plot of the normalized group velocity dispersion for a silica-core fiber. The normalized length z_0 is obtained in meters by dividing the square of the input pulse width in picoseconds by the value from the plot.

$$A = \sqrt{P/P_1}, \tag{8}$$

where

$$P_1 = \frac{nc\lambda A_{\mathrm{eff}}}{16\pi z_0 n_2} \times 10^{-7}\ \mathrm{W}, \tag{9}$$

τ_0 is the pulse width (full width at half-maximum) of the input pulse ($\tau_0 = 1.76t_0$), $D(\lambda)$ or D is the GVD, $D(\lambda)$ in dimensionless units or D in ps-nm/km, n is the refractive index of the core material and n_2 is its nonlinear Kerr coefficient in electrostatic units (1.1×10^{-13} esu for silica), c is the velocity of light (cm/s), and λ is the vacuum wavelength (cm). Figure 10.4 is a plot of the normalized GVD for a silica-core fiber, based on values of $D(\lambda)$ derived from Gloge (1971) and Payne and Gambling (1975). The peak power of the input pulse is given by P, and the quantity A_{eff} is an effective core area (cm^2), which for typical fiber parameters is fairly close to the actual core area. These normalized parameters come out of the theory for optical solitons in fibers (*negative* GVD), where z_0 is the soliton period and P_1 is the peak power of the fundamental soliton (Mollenauer et al., 1980). In the present regime of *positive* GVD there are no solitons, but these parameters are still useful because z_0 is actually the length of fiber required for GVD to approximately double the width of the input pulse (in the *absence* of SPM), and P_1 is the peak power required for SPM to approximately double the spectral width of the input

As discussed earlier, an intense optical pulse will be spectrally broadened and frequency chirped on exiting the fiber. The next step of the pulse compression process is to reassemble the chirped pulse with a compressor. The action of the compressor is most easily described in the frequency domain since it is simply a frequency-dependent time delay. The Fourier transform of the pulse can be expressed in the form

$$\mathcal{E}(z,\omega) = A(\omega)e^{i\phi(\omega)}, \tag{10}$$

where $A(\omega)$ and $\phi(\omega)$ are the amplitude and phase (for simplicity we do not indicate their z dependence explicitly). The effect of the compressor can be described by a phase function $\phi_c(\omega)$, so that the Fourier transform of the compressed pulse is given by

$$\mathcal{E}_c(z,\omega) = A(\omega)\exp\{i[\phi(\omega) + \phi_c(\omega)]\}. \tag{11}$$

If $\phi_c(\omega) = -\phi(\omega)$, then at $t = 0$ all the frequency components of the pulse will be in phase and will thus create the pulse with the maximum peak amplitude. We assume that it is also the shortest possible compressed pulse or close to it. We define this compressor as *ideal*.

One of the most useful types of compressors is the Treacy (1968, 1969) grating-pair compressor. A grating-pair compressor has a delay function that is approximately of the form

$$\phi_c(\omega) = \phi_0 - a_0\omega^2. \tag{12}$$

The compressor constant a_0 can easily be adjusted by varying the grating separation and is thus a directly accessible experimental parameter. We use the term *quadratic* compressor to refer to a compressor with a response function of the form of Eq. (12). It can be shown that the Fourier transform of a pulse with a linear frequency chirp, which means that the temporal phase is proportional to t^2, has a phase that is proportional to ω^2, so that, for a linearly chirped pulse, a quadratic compressor is the *ideal* compressor. To the extent that the frequency chirp on a pulse is nonlinear, a quadratic compressor is not the ideal compressor for that pulse, but if the departure is not too large, a quadratic compressor can still give reasonably good compression. The expression for the grating constant is

$$a_0 = \frac{b\lambda^3}{4\pi c^2 d^2 \cos^2\gamma'}, \tag{13}$$

where b is the center-to-center distance between the two gratings, d is their groove spacing, λ is the center wavelength of the pulse, and γ' is the angle between the normal to the input grating and the diffracted beam at λ. From the numerical solutions of Eq. (5), which includes GVD, Tomlinson et al. (1984) and Stolen et al. (1984c) were able to derive an expression for the grating constant in terms of the input pulse duration and peak amplitude,

$$a_0/t_0^2 \approx \tau/\tau_0 \approx 1.6/A \tag{14}$$

or

$$a_0 \approx 0.52\tau_0^2/A. \tag{15}$$

An expression for the grating separation can also be generated in terms of these experimental parameters by combining Eqs. (13) and (15):

$$b \approx \frac{2.08\pi c^2 d^2 \cos^2\gamma'}{\lambda^3}\left(\frac{\tau_0^2}{A}\right). \tag{16}$$

For the limiting case of zero GVD, the numerical results for the optimum quadratic compressor lead to

$$a_0/t_0^2 \approx 0.25(A^2 z/z_0)^{-1}. \tag{17}$$

Using Eqs. (13) and (17) as well as the pulse length normalization ($\tau_0 = 1.76t_0$), the grating separation in the absence of GVD is given by

$$b \approx \frac{0.323\pi c^2 d^2 \cos^2\gamma'}{\lambda^3}\left(\frac{\tau_0^2}{A^2 z/z_0}\right). \tag{18}$$

It is interesting to discuss the role GVD plays in the pulse compression process. In simulating the compression of picosecond pulses chirped by propagating in the nonlinear Kerr liquid CS_2, Fisher and Bischel (1975) concluded that GVD would have the influence of expanding the temporal region over which the chirp was relatively linear, resulting in optimum compression. Grischkowsky and Balant (1982a, 1982b) were the first to realize the significance of GVD in fiber-grating compression. During passage through the fiber, both the pulse shape and the frequency bandwidth are broadened by the combined action of SPM and positive GVD. Thus, the red-shifted light generated at the leading edge of the pulse travels faster than the blue-shifted light generated at the trailing edge, and this leads to pulse spreading and rectangular pulse shapes. Because the new frequencies are generated primarily at the leading and trailing edges, which gradually move apart in time, the pulse develops a linear frequency chirp over most of the pulse length. These "enhanced frequency chirped" (Grischkowsky and Balant, 1984a, 1984b) pulses can lead to almost ideal compression by a grating pair. Negligible GVD, on the other hand, can lead to large deviations from linearity of the chirp, which can result in substantial wings or sidelobes on the compressed pulse.

Optimum fiber-grating compression requires the appropriate choice of the fiber length and grating spacing for optimum chirp and chirp compensation, respectively. These length scales can vary over an enormous range. For example, Knox et al. (1985) compressed 40-fs pulses to a duration of 8 fs using 7 mm of fiber and a grating separation of approximately 1 cm. On the other extreme, Johnson et al. (1984a, 1984b) compressed 33-ps pulses to a duration of 410 fs using 105 m of fiber and a grating separation of 7.2 m. For a particular input pulse width, peak power, wavelength, and fiber core area, the optimal chirp occurs for a single fiber length. The optimal fiber length

$$z_{opt} \propto \tau_0^2/\sqrt{P}. \tag{19}$$

Not unexpectedly, the grating separation has the same dependence on input pulse width and peak power (see Eqs. (8) and (16)).

Two limiting fiber length regimes of practical interest can be identified (Tomlinson et al., 1984; Stolen et al., 1984). The first is that of a fiber of optimum length to provide the best linear chirp (Grischkowsky and Balant, 1982a, 1982b). The second regime is that for which the length is much less than optimal and the effects of GVD can be neglected. Some of the properties of the chirp and compression in these two limiting regimes are illustrated in Figure 10.5, where the compression factor is about 12.5× in each case. Displayed in Figure 10.5 are the pulse shape exiting the fiber, the frequency spectrum, the chirp, and the compressed pulse for both optimum quadratic and ideal compressors. If GVD is negligible, the fiber output pulse will have the same shape and intensity as the input pulse, while in a fiber of optimum length GVD will broaden the output pulse by about a factor of 3×. As pointed out by Grischkowsky and Balant (1982a, 1982b), a "squared" or "rectangular" fiber output pulse will have a linear frequency chirp over most of the length of that pulse. The overall width of the frequency spectrum is about the same

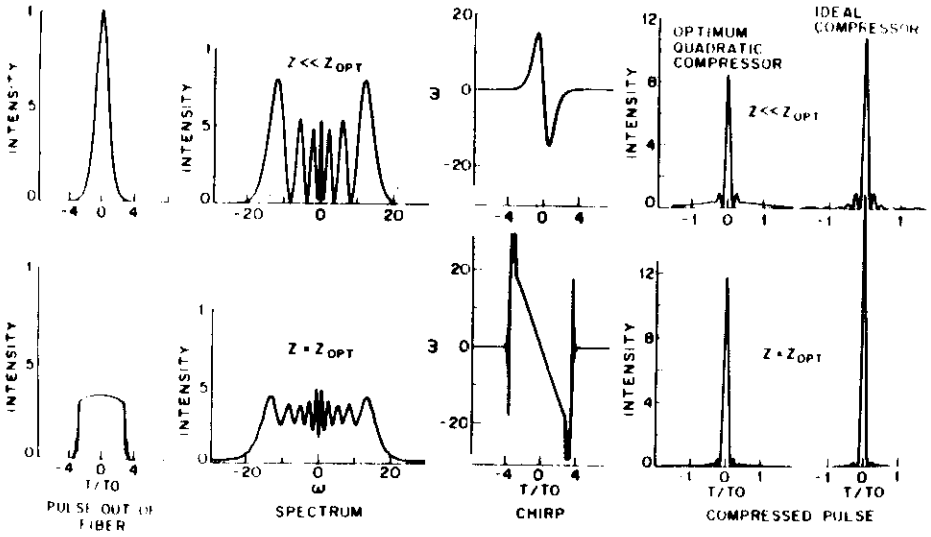

FIGURE 10.5. Pulse shapes before and after grating compression, frequency spectra, and chirp for the limiting regimes of optimal fiber length and of negligible group velocity dispersion. The upper curves are for the case of negligible GVD and an intensity-length product $A^2 z/z_0 = 12.5$. The lower curves are for $A = 20$ and the corresponding optimum fiber length of $z_{opt} = 0.075 z_0$. To compare the quality of compression in the two regimes, a common compression factor of approximately 12.5× was chosen in

TABLE 10.1. Fiber grating compressor parameters.[a]

$$C_1 = \frac{D(\lambda)\lambda}{0.322\pi^2 c^2} = \begin{cases} 0.144 & (\lambda = 0.5145\ \mu m) \\ 0.138\ m^{-1}\ ps^2 & (\lambda = 0.532\ \mu m) \\ 0.117 & (\lambda = 0.600\ \mu m) \\ 0.031 & (\lambda = 1.064\ \mu m) \end{cases}$$

$$P_1 = \frac{nc\lambda A_{eff}}{16\pi z_0 n_2} = 7.92\left[\frac{\lambda(\text{cm})A_{eff}(\text{cm}^2)}{z_0(\text{cm})}\right] \times 10^{14}\ \text{W}$$

$z = z_{opt}$	$z \ll z_{opt}$
$\tau_0/\tau \approx 0.634$	$\tau_0/\tau \approx 1 + 0.9[A^2 z/z_0]$
$z_{opt}/z_0 \approx 1.6/A$	
$b \approx 84 C_2 \frac{\text{cm}}{\text{ps}^2}\left[\frac{\tau_0^2}{A}\right]$	$b \approx 13 C_2 \frac{\text{cm}}{\text{ps}^2}\left[\frac{\tau_0^2}{A^2 z/z_0}\right]$

$$C_2 = \left[\frac{d(\text{cm})}{5.56 \times 10^{-5}}\right]^2 \left[\frac{600}{\lambda(\text{nm})}\right]^3 \cos^2\gamma'$$

[a] $z_0 = \tau_0^2/C_1$; $A = \sqrt{P/P_1}$; $\tau_0 = 1.76 t_0$.

in the two cases, but GVD acts to fill in the spectrum. For each length, the grating separation was optimized to give the maximum peak intensity. The optimum fiber length was chosen to maximize the energy in the compressed pulse. In Figure 10.5 it is interesting to note that when the fiber length and grating separation are optimized, the quality of the compressed pulse (optimum quadratic compressor) is better than that with the ideal compressor in the absence of GVD.

The procedure of Tomlinson et al. (1984) and Stolen et al. (1984c) for calculating the compression, the optimal fiber length, and the grating separation is presented in Table 10.1. There are two important normalized parameters. The first is the normalizing length z_0 defined in Eq. (7), and the second is the normalized amplitude A defined in Eq. (8). For a silica-core fiber the GVD parameter C_1 has been given for several common laser wavelengths but can also be read directly from Figure 10.4 for an arbitrary wavelength. Table 10.1 also gives approximate expressions for the compression factor τ_0/τ, the optimum fiber length z_{opt}, and the grating separation b in both limits of fiber length (see Eqs. (16) and (18)). These expressions are supported by a recent approximate analytical theory of the compression process reported by Meinel (1983). The angle γ' is between the normal to the grating and the diffracted beam. For $A \leq 3$, the compression and pulse quality are not strong functions of fiber length, so there is no clear optimum length. This fact is consistent with the results of Shank et al. (1982) in which 90-fs pulses were compressed with fiber lengths between 4 and 20 cm and produced the same factor of 3× compression.

Johnson et al. (1984a, 1984b) used these numerical calculations to design

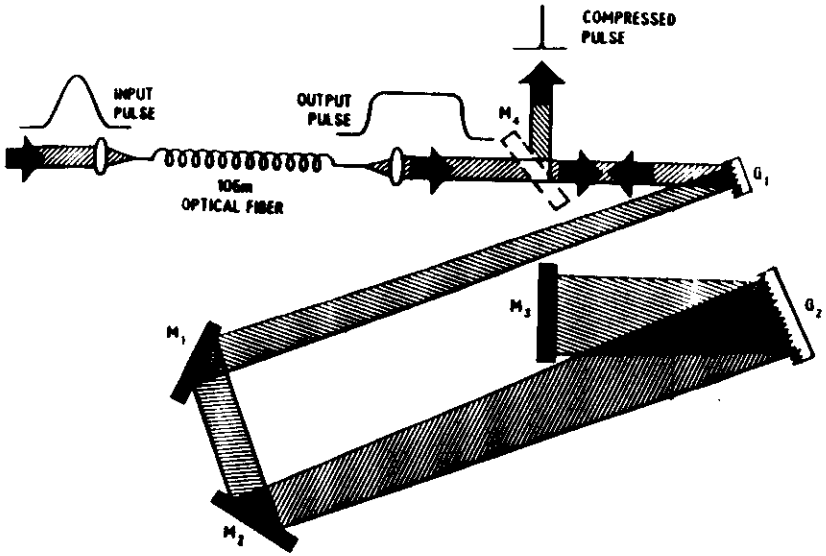

FIGURE 10.6. Schematic drawing of the "double-pass" fiber-grating pulse compressor used for the 80 × compression of 0.532-μm pulses. The dispersive delay line consists of gratings G_1 and G_2 (1800 grooves/mm) and mirrors M_1, M_2, and M_3. Mirror M_4 is cut in half to allow the fiber output pulse to pass over it. M_3 is slightly tilted downward to allow the output beam to be reflected by M_4 out of the compressor. The round-trip distance between the gratings was 724 cm.

a frequency-doubled Nd:YAG laser. The calculation deduced an optimum fiber length $z_{opt} = 83$ m, a grating separation $b = 606$ cm (1800 grooves/mm), and a compressed pulse width $\tau = 350$ fs. The experiment consisted of coupling 240-W pulses into a 105-m single-mode polarization-preserving fiber (Stolen et al., 1978) with a core diameter of 3.8 μm. A schematic drawing of the fiber-grating compressor is displayed in Figure 10.6. Compressed pulses as short as 410 fs or a compression of 80 × was obtained with a grating separation of 724 cm. The fiber input pulse and the compressed pulse are displayed together in Figure 10.7. The agreement between calculation and experiment was quite remarkable in light of the fact that the calculations were for normalized amplitudes of $A \leq 20$. The compression experiments had normalized amplitudes of $A > 150$.

As a result of the limited availability of high-reflectivity gratings at 0.532 μm with greater groove densities than 1800 grooves/mm it was important to keep the input pulse width as short as possible to avoid an unreasonable grating separation. The grating separation varies as the square of the input pulse width (see Eq. (16)). This is not as serious a problem at 1.064 μm, where the cubic wavelength dependence is quite helpful in keeping

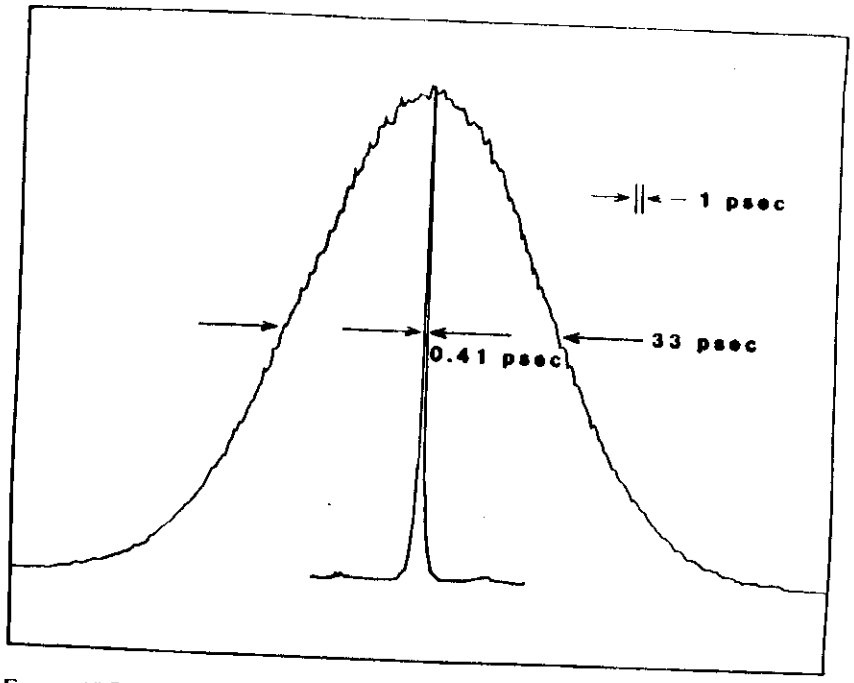

FIGURE 10.7. 80 × compression of 33-ps, 0.532-μm pulses. Standard background-free autocorrelation of the input and compressed pulses displayed on the same scale. (Input: Gaussian pulse shape. Compressed pulse: sech^2 pulse shape.)

the grating separation reasonable. The 33-ps fiber input pulses were obtained by frequency doubling a harmonically mode-locked CW Nd:YAG laser (Johnson and Simpson, 1983, 1985a; Keller et al., 1988). As opposed to fundamental mode locking, typical harmonic mode-locked pulse widths are 50 ps at 1.064 μm (Johnson and Simpson, 1985a) (see Figure 10.8). If 50- to 60-ps fiber input pulses (0.532 μm) from a standard fundamentally mode-locked laser were used, a grating separation of greater than 14 m would have been needed.

At this point it is useful to give a pulse compression example replete with experimental parameters, numerical calculation parameters, and the resultant numerical simulation of the compression process. This next example of 0.532 μm pulse compression was performed using a separate, larger-core fiber distinct from that discussed earlier in Johnson et al. (1984a, 1984b). A "flat" polarization-preserving fiber made by preform deformation (Stolen et al., 1984b) with a 4.1-μm silica-core diameter. A micrograph of the fiber is shown in Figure 10.9. The birefringence resulting from the stress cladding lifts the degeneracy of the two orthogonal modes of propagation. Thus linearly polarized light propagating along the well-defined principal fiber axis will be

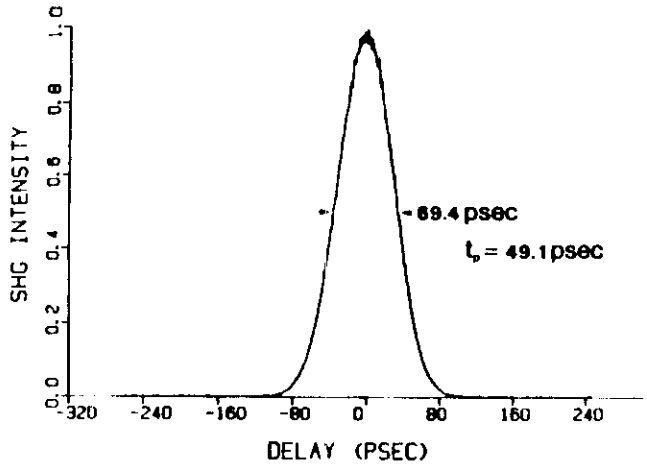

FIGURE 10.8. Background-free autocorrelation of the 1.064-μm output of a harmonically mode-locked CW Nd:YAG laser (Gaussian pulse shape). These pulses are frequency doubled in $KTiOPO_4$ (KTP) to yield pulses of 33 to 35 ps duration at 0.532 μm.

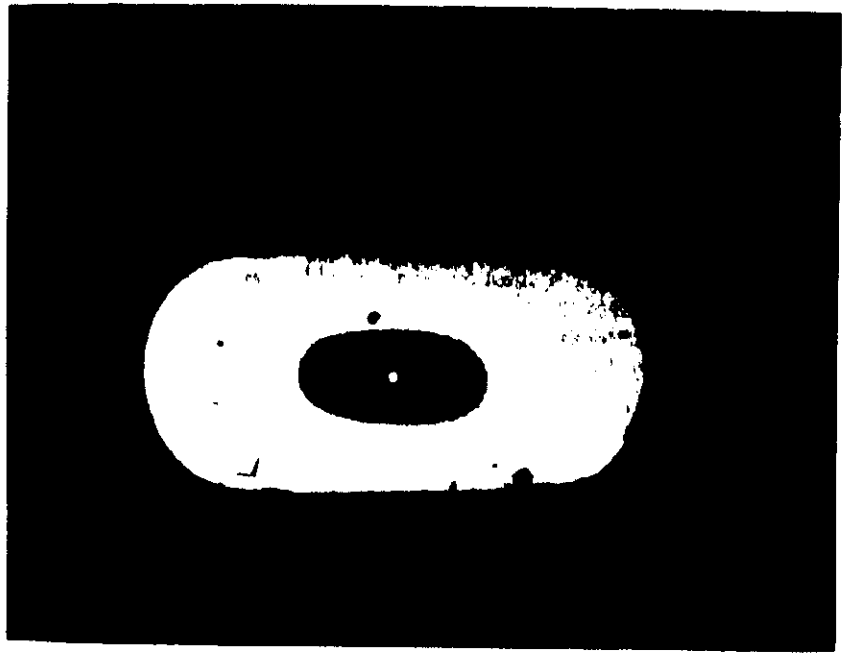

FIGURE 10.9. "Flat" polarization-preserving fiber made by preform deformation. The 4.1-μm pure silica core is surrounded by a $B:Ge:SiO_2$ stress cladding, an $F:SiO_2$ outer cladding, followed by a pure silica support cladding. The "rectangular" fiber has over-

preserved. The diffraction efficiency of the gratings is a very sensitive function of the polarization of the fiber output. Thus, polarization-preserving fiber is extremely useful in reducing amplitude fluctuations in the compressed output due to polarization "scrambling" effects in fibers. One disadvantage of using polarization-preserving fibers is that the threshold for stimulated Raman scattering (SRS) is reduced by a factor of 2 in fibers maintaining linear polarization (Stolen, 1979a). Experimentally, it was found that the reduced SRS threshold was a small price to pay for the increased amplitude stability afforded by polarization-preserving fiber. The effects of SRS on compression are discussed in the next section.

For comparable compression, this larger core diameter fiber resulted in the reduction of SRS by about a factor of 2. The fiber length was 93.5 m and had a loss of 16 db/km at 0.532 μm. At the input lens (10× objective) the peak power was 235 W (820 mW average, 100 MHz repetition rate). However, this is not the best estimate of the peak power actually coupled into the fiber. The best approach is to measure the light coupled out of the fiber and correct for the transmission of the output lens and the known loss in the given length of fiber. This approach corrects for the loss in the input lens, mode-matching effects, light coupled into the cladding, and the reflection loss on the the fiber input face. In this instance the peak power actually coupled into the fiber is closer to 172 W. The fiber-grating compressor parameters given in Table 10.1 can be calculated with the following information: $P = 172$ W, $\tau_0 = 35$ ps, $n = 1.46$, $A_{\text{eff}} = 0.92A_{\text{core}} = 1.21 \times 10^{-7}$ cm^2, $n_2 = 1.1 \times 10^{-13}$ esu, $P_1 = 5.74$ mW, $A = 173$, $z_0 = 8.88$ km, $d = 5.56 \times 10^{-5}$ cm, and $\gamma' = 32.5°$. The calculations indicate an optimum fiber length $z_{\text{opt}} = 82$ m, a grating separation of 603 cm, and a compressed pulse width of 320 fs. With this fiber, pulses have been compressed to durations as short as 430 fs (80× compression). The typical day-to-day duration of the compressed pulses falls in the range 460 to 470 fs (Johnson and Simpson, (1985a, 1986). The actual grating separation used to generate the 460-fs pulse,displayed in Figure 10.10 was 698 cm.

What actually happened to the 35-ps, 235-W pulse as it propagated through the fiber-grating compressor to produce the clean 460-fs pulses at the output? The spectral width of the fiber input pulses was measured to be 0.27 Å and was limited by the slits on the spectrometer. The self-phase-modulated spectrum of the output pulse was broadened to 17.2 Å and is displayed in Figure 10.11. GVD acted to fill in the self-phase-modulated spectrum, resulting in a flattened spectrum. The fiber output pulse was substantially broadened to a duration of 142 ps and is displayed in Figure 10.12. The triangular autocorrelation function is indicative of a rectangular intensity profile. As pointed out by Grischkowsky and Balant (1982a, 1982b), a rectangular fiber output pulse will have a linear frequency chirp over most of its length and result in optimum compression by a grating pair.

The two symmetrically located sidelobes on the fiber output frequency spectrum in Figure 10.11 are not expected from pure SPM. To determine

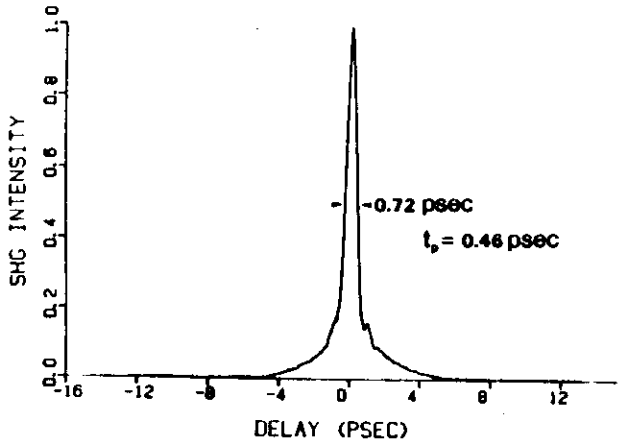

FIGURE 10.10. Typical autocorrelation of the compressed 0.532-μm pulses using a 93.5-m length of the "flat" polarization-preserving fiber displayed in Figure 10.9. Typical day-to-day pulses fall into the range of 460 to 470 fs.

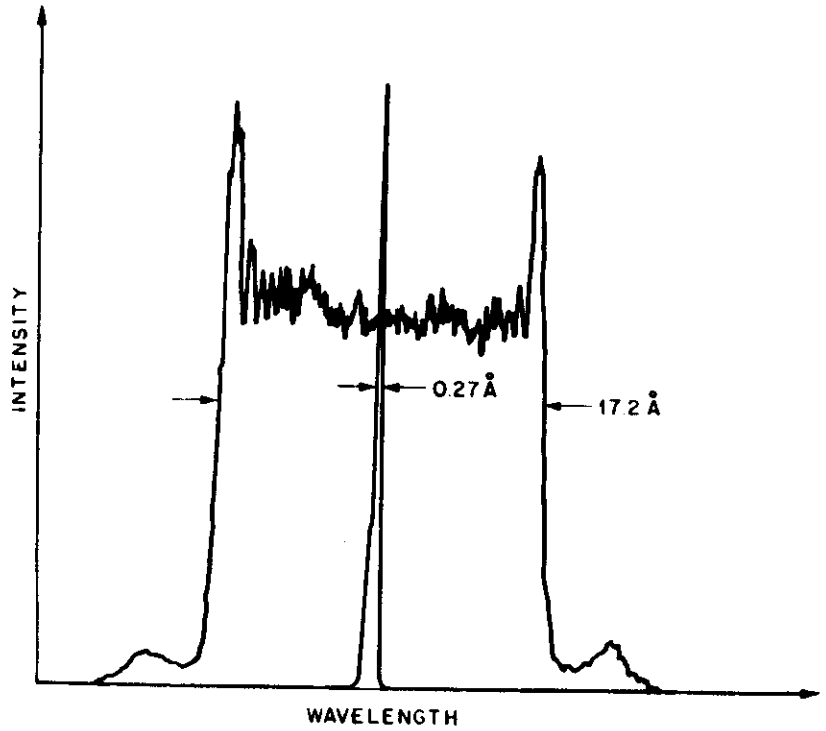

FIGURE 10.11. Spectral width of the 35-ps, 235-W, 0.532-μm fiber input pulses and the spectrally broadened (by SPM) output pulses after propagation down a 93.5-m length of the 4.1-μm core diameter polarization-preserving fiber.

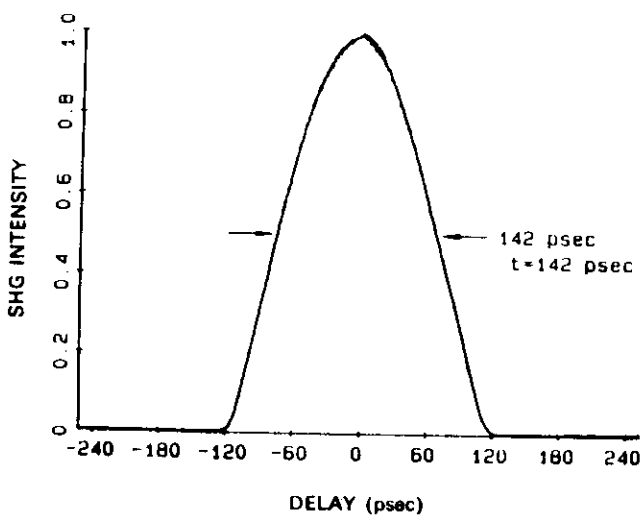

FIGURE 10.12. Autocorrelation of the fiber output pulse broadened by GVD. A triangular autocorrelation function is indicative of a rectangular intensity profile that has a deconvolution factor of unity.

simulations of the nonlinear pulse propagation using the experimental and calculated numerical parameters given previously. The results of several of the numerical calculations are given in Figure 10.13. This figure presents the nonlinear pulse propagation as a function of fiber length z/z_0. In Figure 10.13a, at $z/z_0 = 0.0020$ ($z = 18$ m), the temporal shape of the pulse is only slightly broadened (the input pulse width is $1.76t_0$), and the instantaneous frequency function and spectrum are characteristic of pure SPM. Recall that the calculated optimum fiber length is $z_{opt} = 82$ m. In Figure 10.13b, at $z/z_0 = 0.0054$ ($z = 48$ m), the temporal shape has become more "rectangular" as a result of the influence of GVD. The instantaneous frequency function indicates a nearly linear frequency chirp over a significant portion of the pulse width. In Figure 10.13c, at $z/z_0 = 0.0060$ ($z = 53$ m), as the fiber length approaches z_{opt} the chirp "linearization" proceeds as a result of the concomitant pulse broadening.

Figure 10.14 displays the instantaneous frequency function, the temporal pulse shape, and its frequency spectrum, for a length $z/z_0 = 0.01$ ($z = 89$ m), for a lossless fiber and for a fiber with a loss of 16 db/km (normalized loss parameter $\alpha = 16.36$). The nonlinear Schrödinger equation (Eq. (5)) with the inclusion of a normalized linear loss parameter α is given by

$$\frac{\partial \mathscr{E}}{\partial(z/z_0)} = -i\frac{\pi}{4}\left[\frac{\partial^2 \mathscr{E}}{\partial(t/t_0^2)} - 2|\mathscr{E}|^2\mathscr{E}\right] - \alpha\mathscr{E}. \tag{20}$$

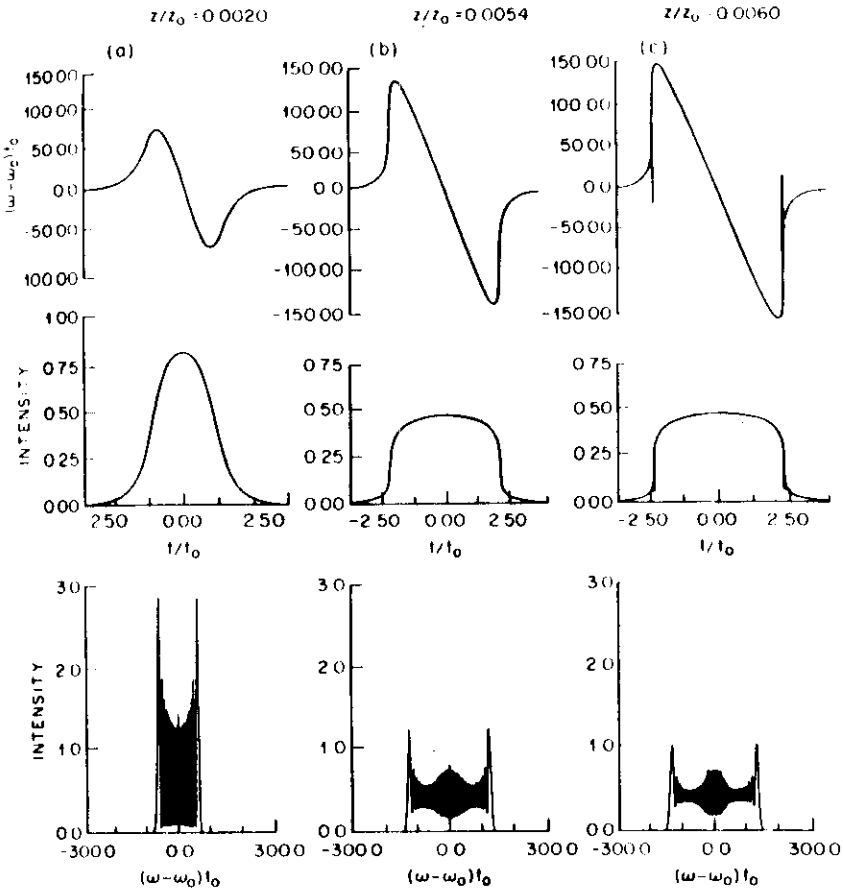

FIGURE 10.13. Numerical simulations of the nonlinear pulse propagation of 34.4-ps pulses (t_0 = 19.5 ps) at 0.532 μm with a normalized input amplitude of A = 173 and normalizing fiber length of z_0 = 8.88 km displayed as a function of fiber length z/z_0. The upper curves show the instantaneous frequency as a function of time, the middle curves show the intensity as a function of time, and the lower curves show the frequency spectra of the pulses. For the 93.5-m fiber used the normalized length was $z/z_0 = 0.0105$.

In Figure 10.14a and b the resulting pulse shape shows well-developed interference fringes on the leading and trailing edges. The frequency spectra clearly display the symmetrically located sidelobes. The spectrum for the fiber with loss (Figure 10.14b) is in excellent agreement with the experimental spectrum of Figure 10.11. (Since the experimental spectrum is an average over many pulses, we do not expect to see the fine structure displayed in the calculated spectrum.) Simulations of the effect of a grating-pair compressor on these fiber output pulses gave a compression of 98 × for the lossless fiber and of 84 ×

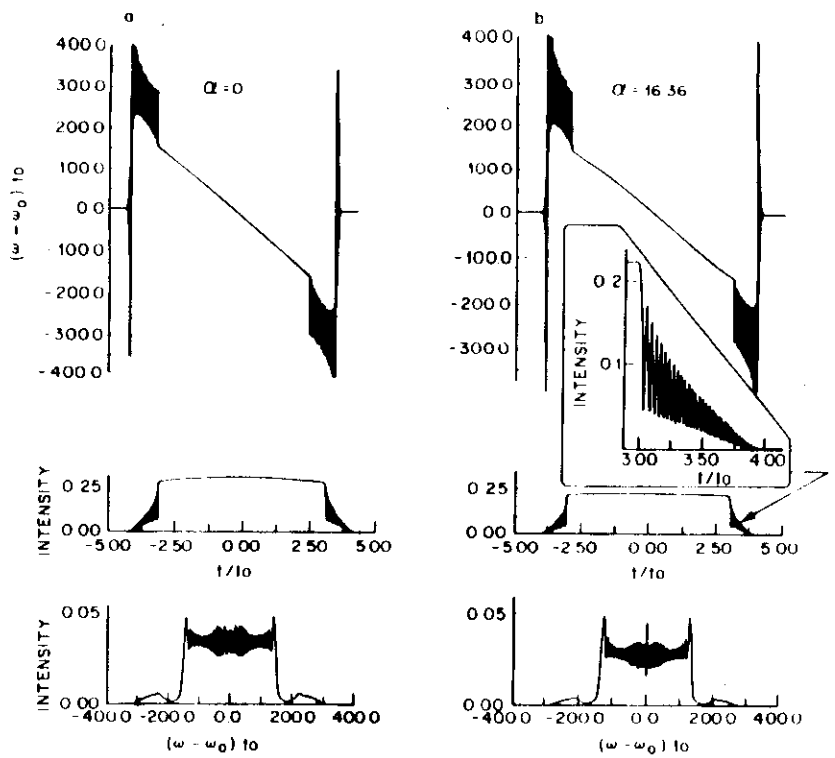

FIGURE 10.14. Numerical simulations of nonlinear pulse propagation for A = 173 and a fiber length of z/z_0 = 0.01 for (a) a lossless fiber and (b) a fiber with a normalized loss parameter α = 16.36 (16 db/km). The upper curves are the instantaneous frequency, the middle curves are the temporal shape of the output pulse, and the lower curves show the frequency spectra of the output pulses. The inset in (b) displays a detail of the interference region (optical wave-breaking) on the edge of the pulse.

for the fiber with loss. Thus by including the fiber loss in the nonlinear Schrödinger equation, numerical solutions of Eq. (20) are in excellent agreement with the experimentally observed 80 × compression.

The origin of the sidelobes in the frequency spectrum of the fiber output pulses on Figures 10.11 and 10.14 has been attributed to a phenomenon that Tomlinson et al. (1985) dubbed "optical wave-breaking." Briefly, when an intense pulse propagates down an optical fiber, the leading edge of the pulse experiences a frequency decrease or red shift, while the trailing edge experiences a blue shift. For large-compression experiments (large values of the normalized amplitude A) in the presence of GVD, the red-shifted light near the leading edge of the pulse travels faster than, and overtakes, the unshifted light in the forward tails of the pulse (and vice versa on the trailing edge). Therefore, the leading and trailing regions of the pulse will contain light

at two different frequencies, which will interfere and generate new frequencies. These new frequencies appear as the sidelobes on the fiber output spectrum and result in a small increase in the background on the compressed pulse. This phenomenon is somewhat analogous to the "breaking" of water waves and has been described as optical wave-breaking. Optical wave-breaking can also occur in small-compression-ratio experiments (small values of A) if the fiber is longer than the optimum fiber length, so that there is sufficient GVD to mediate the interference process. The interference fringes resulting from the optical wave-breaking are prominent in the calculated temporal pulse shapes (see inset of Figure 10.14b). Since the spectral bandwidth that contributes to the compressed pulse is approximately twice the frequency difference involved in the wave-breaking interference, the period of the interference fringes is approximately twice the width of the compressed pulse. Additional evidence for optical wave-breaking has appeared in the numerical studies of nonlinear pulse propagation by Lassen et al. (1985).*

These experiments and numerical simulations demonstrate the enormous range of applicability of the nonlinear Schrödinger equation (Eq. (20)) for describing nonlinear pulse propagation in single-mode fibers. Each of the various terms in Eq. (20) represents the lowest-order approximation to the phenomenon that it is describing, and it is assumed that the higher-order terms will be significant for very high compression ratios and/or very short input pulses. The present results indicate that large compression ratios of 80 × can accurately be described by Eq. (20) without invoking any higher-order terms. The limits of this fiber-grating compression approach have recently been studied by Bourkoff et al. (1987a, 1987b), Tomlinson and Knox (1987), and Golovchenko et al. (1988).

2.3 Stimulated Raman Scattering and Pulse Compression

The interplay between optical fiber pulse compression ($\lambda < 1.3$ μm) and stimulated Raman scattering, or more appropriately the interplay between SPM, SRS, and GVD, could easily fill a book chapter. It is much beyond the scope of this chapter to discuss the role of SRS in great detail. Instead, the reader is referred to a number of excellent articles on SRS and nonlinear pulse propagation in fibers in the region of positive GVD: Auyeung and Yariv, 1978; Butylkin et al., 1979; Dianov et al., 1984b, 1985, 1986a, 1987; Gomes et al., 1986a, 1986b, 1988a; Heritage et al., 1988; Hian-Hua et al., 1985; Johnson et al., 1986; Kuckartz et al., 1987, 1988; Lin et al., 1977; Nakashima et al., 1987; Ohmori et al., 1983; Roskos et al., 1987; Schadt et al., 1986, 1987; Smith, 1972; Stolen and Ippen, 1973; Stolen and Johnson, 1986; Stolen et al., 1984a, 1972; Stolz et al., 1986; Valk et al., 1984, 1985; Weiner et al., 1988. Several of the salient features of SRS are briefly discussed in this section.

* Note added in proof: Optical wave-breaking was recently observed (temporally) by Rothenberg and Grischkowsky (1989).

The maximum power of an optical pulse in a fiber is usually limited by SRS. In the region of positive GVD, a Raman Stokes pulse will travel faster than the pump pulse. Thus the role of GVD is important in determining the limitations of SRS on the self-phase-modulated pump pulse. Stolen and Johnson (1986) discussed a simple picture of the SRS process that assumes that the Stokes power builds up from a weak injected signal rather than from spontaneous scattering. This follows the approach of Smith (1972) for CW Raman generation, in which the integrated spontaneous Raman scattering along the fiber can be replaced by a weak effective Stokes input power. At the top of Figure 10.15, a portion of the injected CW Raman signal enters the fiber along with the leading edge of the pump pulse. Because of GVD, this part of the signal will travel faster than the pump and never experience Raman amplification. In the second line of Figure 10.15, a portion of the signal enters the fiber along with the peak of the pump pulse. As the pump pulse travels along the fiber with velocity V_p, the faster-traveling Stokes signal (V_s) is amplified by extracting energy from the pump. Amplification ceases when the signal has passed through the pump pulse. Maximum amplification will occur for a Stokes signal that passes through the entire pump pulse, and this is the portion of the CW signal that enters the fiber along with the trailing edge of the pump pulse (third line of Figure 10.15). If a significant part of the pump energy has been shifted to the Stokes frequency (pump depletion), subsequent portions of the CW signal (fourth and fifth lines of Figure 10.15) will see a much reduced amplification.

The net result is that the amplification of the injected CW signal by the pump pulse has produced a Stokes pulse with a peak that is ahead of the pump pulse by about one pump pulse length (line 7 of Figure 10.15). If we define a walk-off length l_w,

$$l_w = \left(\frac{V_s V_p}{V_s - V_p}\right)\tau_0, \tag{21}$$

as the distance in which the Stokes signal passes through one pump pulse width τ_0 the Stokes maximum will be produced about two walk-off lengths into the fiber. All of the Stokes conversion will occur within about four walk-off lengths.

The signal gain depends on distance (L) along the fiber, and the net amplification involves an integral over the region where the Stokes and pump pulses interact. In the limit where the Stokes signal sees the entire pump pulse the gain becomes

$$P(L) = P(0)e^{G}, \tag{22a}$$

$$G \to \frac{g_0 P_0}{A_{\text{eff}}} \int dz \exp\left[-\frac{1.67z}{l_w}\right]^2 = 1.06\frac{g_0 P_0 l_w}{A_{\text{eff}}}, \tag{22b}$$

where g_0 is the peak Raman gain coefficient, A_{eff} is the effective core area, and P_0 is the peak pump power. Thus, the maximum gain is approximately the peak power times the walk-off length. Typical values of G [illegible]

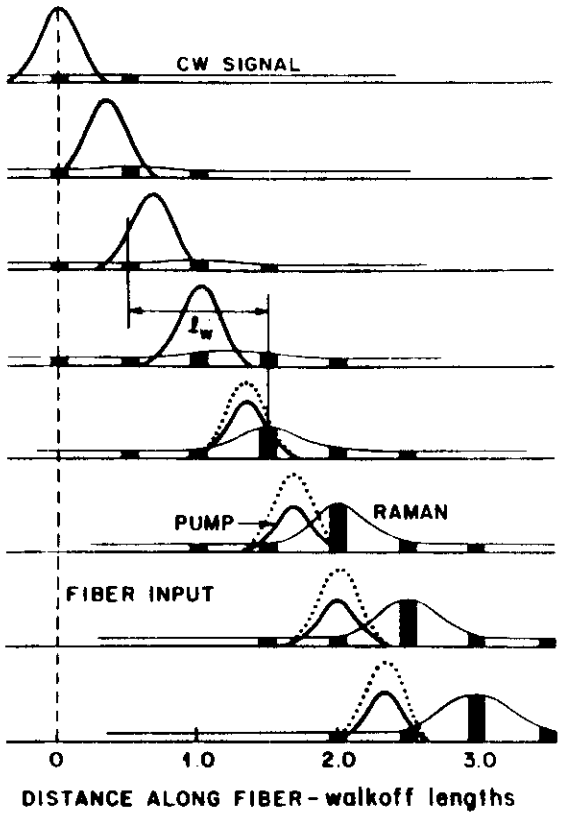

FIGURE 10.15. Schematic representation of a CW Stokes signal amplified as it passes through a pump pulse because of GVD. Portions of the CW signal are separately identified to illustrate that maximum amplification occurs for the part of the CW signal that enters the fiber with the trailing edge of the pump pulse. Earlier portions of the CW signal see reduced gain because they do not pass through the entire pump pulse, and later portions of the signal see reduced gain because the pump pulse has been depleted by earlier Raman conversion. The dotted curve represents the propagation of the pump pulse in the absence of Raman conversion.

but can go as high as 20 for significant Raman conversion and small walk-off or interaction lengths. For example, Stolen and Johnson (1986) estimated a value of $G = 19.7$, for 20% Raman conversion of 35-ps, 0.532-μm pulses, and a walk-off length of 6.2 m.

An estimate of the critical pump power $P_p = P_c$ entering the fiber, for which the intensities of the first Stokes component of SRS and of the pump were equal at the fiber output, was derived for the case of CW SRS by Smith (1972).

This approach has proved to be fairly reliable even in the pulsed case. For the case of *polarization-preserving* fiber, the critical pump power is estimated to be

$$P_c \approx \frac{GA_{\text{eff}}}{g_0 l_w}, \tag{23}$$

and for *non-polarization-preserving* fiber the critical pump power is

$$P_c \approx 2\frac{GA_{\text{eff}}}{g_0 l_w}. \tag{24}$$

The Raman gain in fibers is a factor of 2 higher if linear polarization is maintained (Stolen, 1979) and accounts for the factor of 2 in Eqs. (23) and (24). The peak Raman gain coefficient g_0 at a pump wavelength of 0.526 μm is 1.86×10^{-11} cm/W (Stolen and Ippen, 1973). The Raman gain varies linearly with pump frequency and the peak coefficient for a 1.064-μm pump is $g_0 = 0.92 \times 10^{-11}$ cm/W (Lin et al., 1977).

Fiber-grating compression of optical pulses can be strongly affected by SRS, which at high intensities will distort the pulse profile and consequently the chirp on the pulse. SRS limits the power available in the compressed pulse. Above the Raman threshold, further increases in pump power result only in increased Raman conversion. SRS does not seem to have a major effect on the compression of femtosecond pulses, and this can be attributed to the very short walk-off lengths involved (see Eqs. (21), (23), and (24)). Longer pulses translate into longer walk-off lengths and lower critical powers for the onset of SRS. The compression of the fundamental and the second harmonic of mode-locked Nd:YAG lasers falls squarely into this region of competition between SRS, SPM, and GVD. Under conditions of walk-off of the generated Stokes pulse, intense SRS will preferentially deplete the leading edge of the pump pulse and steepen its rising edge. SPM of the reshaped pump pulse causes nonsymmetric spectral broadening and a nonlinear chirp. An example of the distortion of the self-phase-modulated pump spectrum by the presence of 20% Raman conversion (Stolen and Johnson, 1986) is displayed in Figure 10.16. This figure shows the Stokes and pump spectra for 35-ps, 0.532-μm pump pulses after propagation down 101 m of single-mode polarization-preserving fiber (walk-off length = 6.2 m). The long-wavelength component, or red-shifted frequency component, shows signs of depletion. The resultant nonlinear chirp, of course, leads to very poor fiber-grating compression.

In general, compression in the presence of strong SRS using fiber lengths less than z_{opt} (i.e., negligible GVD) results in compressed pulses accompanied by broad wings. In addition, the spectral fluctuations lead to severe fluctuations in compressed pulse amplitude and shape. Recently, Weiner et al. (1988) demonstrated that high-quality stabilized compression could be achieved, under these circumstances, only by utilizing an asymmetric spectral window (Heritage et al., 1985a) to select out a linearly chirped portion of the broadened spectrum.

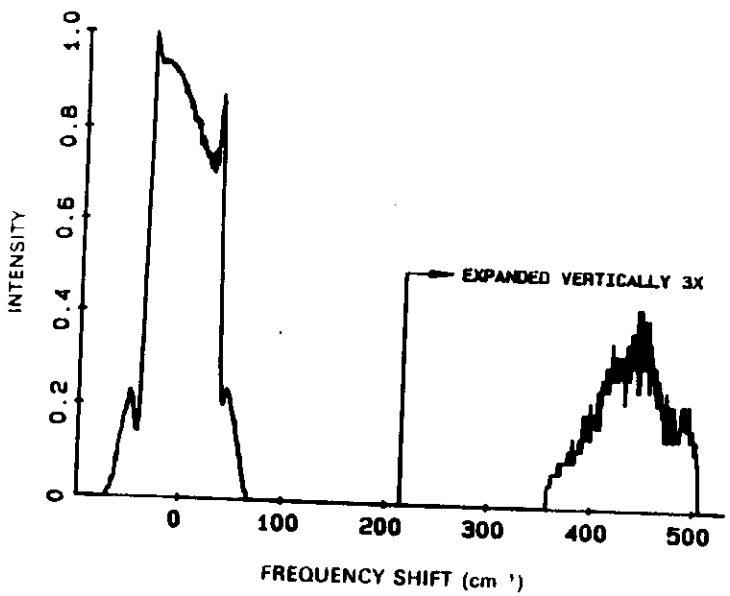

FIGURE 10.16. Raman and pump spectra of 35-ps, 0.532-μm pulses as measured from a 101-m fiber at about 20% Raman conversion. The self-phase-modulated pump spectrum shows signs of depletion of the long-wavelength or red-shifted frequency components by SRS leading to a nonlinear chirp. (Walk-off length = 6.2 m.)

Another approach to obtaining high-quality stable pulse compression is to avoid or severely limit SRS and use fibers of length z_{opt} to obtain the necessary linear chirp. Johnson et al. (1984a, 1984b) generated high-quality 410-fs pulses (80× compression) at 0.532 μm with a fiber length greater than z_{opt} and less than 5% Raman conversion. Using fibers of nearly optimum length and operating below the Raman threshold, Roskos et al. (1987) and Dianov et al. (1987) generated high-quality pulses as short as 550 fs (110× compression) at 1.064 μm.

Earlier pulse compression calculations for shorter fiber lengths clearly indicated that the chirp would be severely distorted and asymmetric as a result of strong SRS (Schadt et al., 1986; Schadt and Jaskorzynska, 1987; Kuckartz et al., 1987). However, Kuckartz et al. (1988) recently demonstrated that in sufficiently long fibers the combined action of GVD and SPM could cause a further reshaping and linearization of the chirp, which then could be efficiently compressed by a grating pair. High-quality pulses with comparatively low substructure as short as 540 fs (130× compression) at 1.064 μm using 120 m of polarization-preserving fiber were obtained in the presence of strong SRS (Kuckartz et al., 1988). Heritage et al. (1988) recently demonstrated that with a 400-m length of polarization-preserving fiber, significant *third* Raman

Stokes generation, and an asymmetric spectral window (Heritage et al., 1985a), high-quality ultrastable compressed pulses as short as 550 fs (130× compression) at 1.064 μm could be obtained. They found that most of the pump spectrum was linearly chirped by the strong reshaping due to strong SRS, SPM, and GVD.

Several review and extended-length articles on nonlinear pulse propagation, pulse shaping, and compression in fibers have recently been published: Alfano and Ho, 1988; Dianov et al., 1988; Golovchenko et al., 1988; Gomes et al., 1988b; Kafka and Baer, 1988; Thurston et al., 1986; Zhao and Bourkoff, 1988. (See Chapter 3.) This list of articles is by no means complete and furthermore is limited to discussions in the region of positive GVD.

Thus far, this chapter has dealt with negative dispersive delay lines consisting of Treacy, (1968, 1969) grating pairs in reflection mode. Several alternatives to this approach deserve mentioning. Yang et al. (1985) demonstrated femtosecond optical fiber pulse compression using a holographic volume phase transmission grating pair. Prisms were used as negative dispersive delay lines by Fork et al. (1984), Martinez et al. (1984), and Bor and Racz (1985) and were used in femtosecond optical fiber pulse compression by Kafka

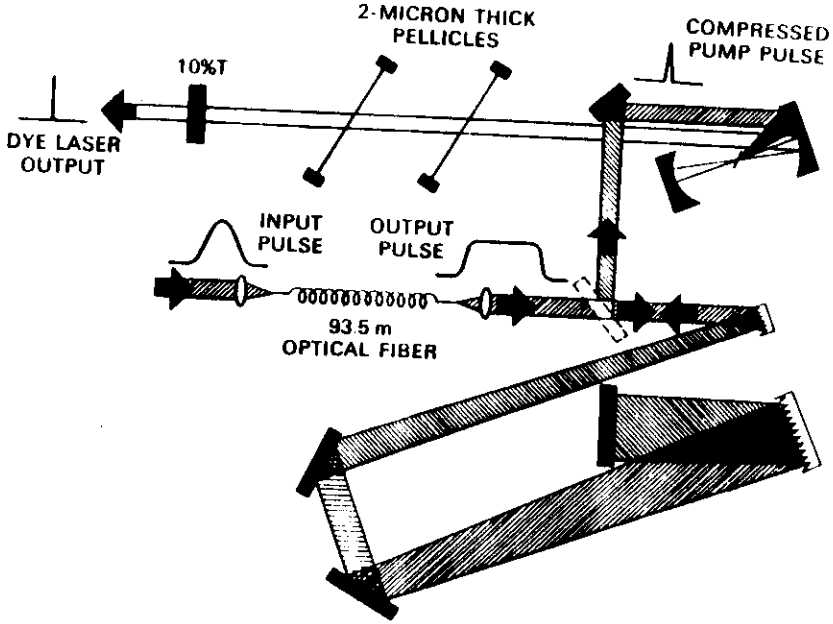

FIGURE 10.17. Schematic of a synchronously mode-locked Rhodamine 6G dye laser pumped by fiber-grating compressed 0.532-μm pulses. A pair of 2-μm-thick pellicles or a single-plate birefringent filter was used for wavelength tuning and bandwidth control.

and Baer (1987). In another variation, Nakazawa et al. (1988) used a TeO_2 acousto-optic light deflector and corner cube combination as a negative dispersive delay to demonstrate femtosecond optical fiber pulse compression.

One of the first applications of "long" fiber-grating compressed pulses was their use by Johnson et al. (1984b), Johnson and Simpson (1985a, 1985b, 1986), Kafka and Baer (1985, 1986), and Beaud et al. (1986) as a source of ultrashort pump pulses for wavelength-tunable femtosecond dye lasers. A schematic of a Rhodamine 6G synchronously mode-locked dye laser pumped by compressed 0.532-μm pulses is displayed in Figure 10.17. Wavelength-tunable pulses as short as 180 fs (Johnson and Simpson, 1986) were obtained from the dye laser synchronously pumped with 470-fs-duration 0.532-μm pulses (see Figure 10.18).

Johnson et al. (1984a, 1984b) reported that the duration and functional form of the compressed 0.532-μm pulses were extremely sensitive to the grating separation (for constant fiber input power). As the grating separation was decreased from its optimum, the compressed pulse would broaden smoothly. Compressed pulses of 460 to 470 fs (Johnson and Simpson, 1985a) duration were obtained with a grating separation of 698 cm (see Figure 10.10). By decreasing the grating separation by 4.2, 15.6, and 27% the compressed pulses were broadened to 920 fs, 12.3 ps, and 22 ps, respectively (see Figure 10.19).

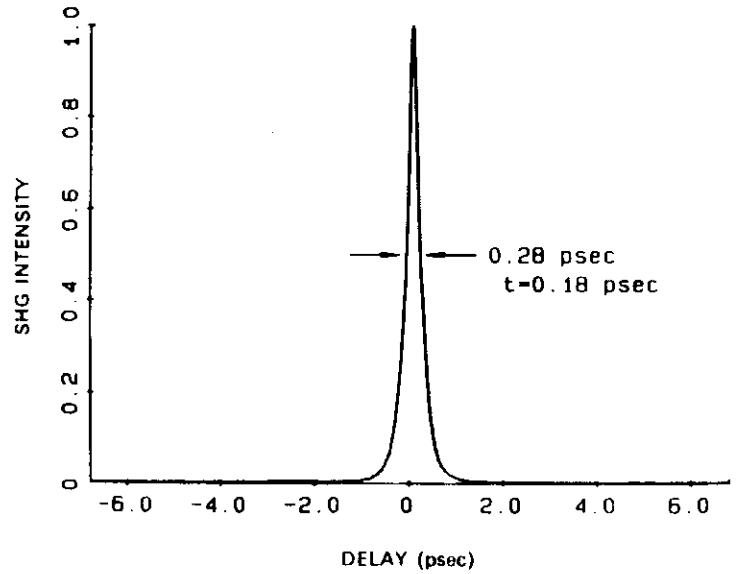

FIGURE 10.18. Autocorrelation function of the pellicle-tuned dye laser synchronously pumped by 470-fs-duration 0.532-μm pulses, tuned to a wavelength of 0.592 μm (sech^2 pulse shape assumed).

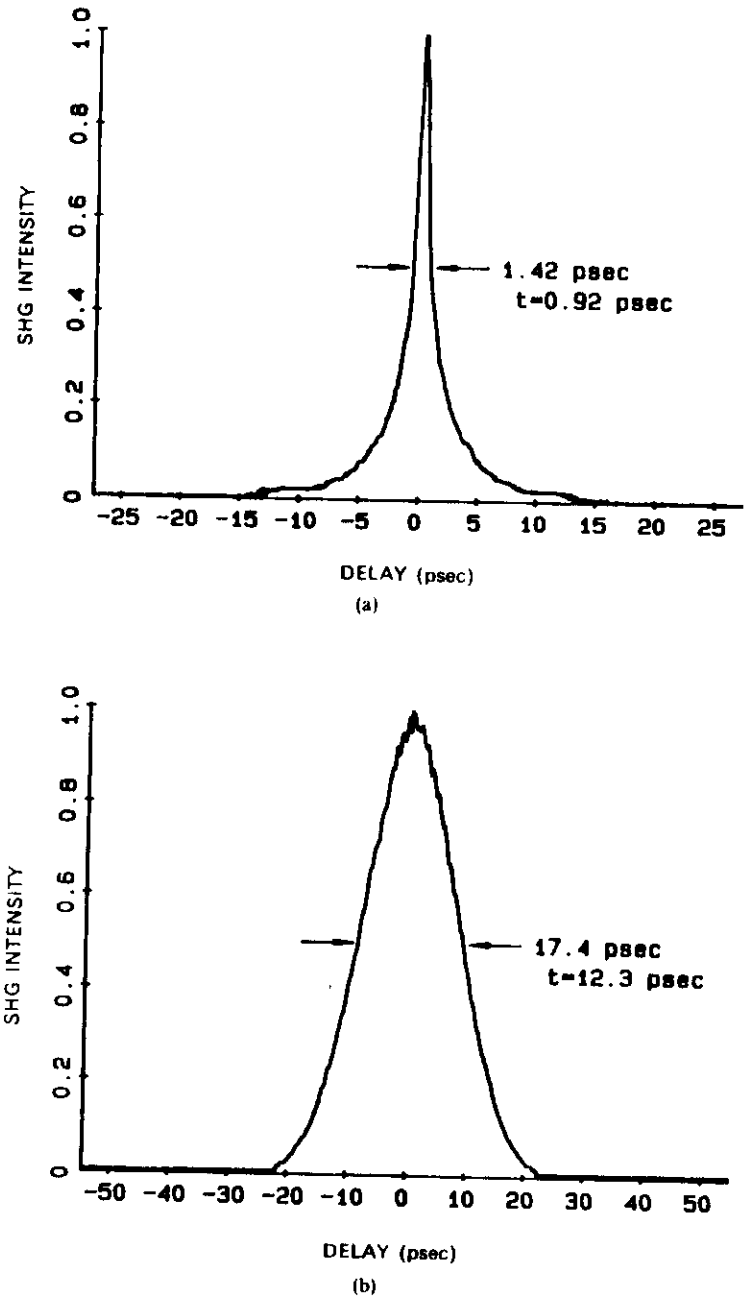

FIGURE 10.19. *Temporal* tuning of compressed 0.532-μm pulses with decreasing grating separation from the optimum (see Figure 10.10). The grating separation was reduced from the optimum of 698 cm by (a) 4.2% (sech^2 pulse shape), (b) 15.6% (Gaussian pulse shape, and (c) 27% (Gaussian pulse shape).

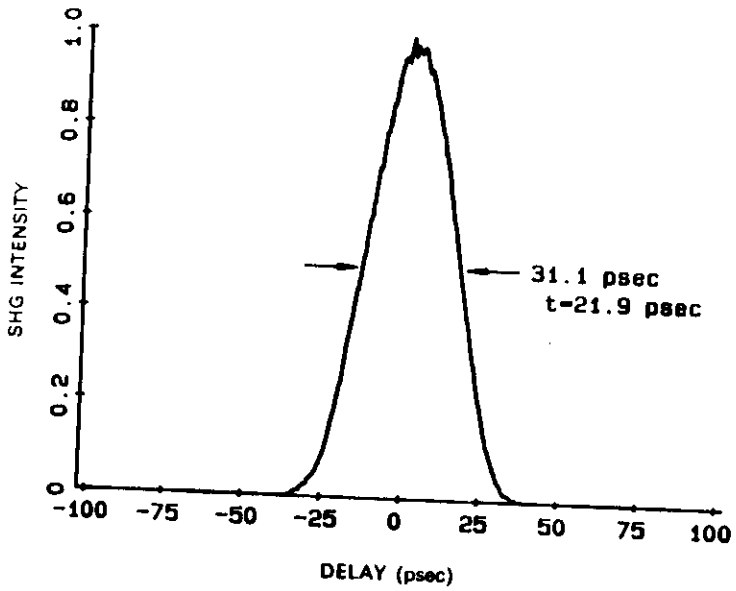

(c)

FIGURE 10.19 (*continued*)

Thus a *temporally* tunable source of ultrashort pulses was demonstrated. With this source of temporally tunable pump pulses, the first reported investigation of the dynamics of synchronous mode locking as a function of pump pulse duration was made by Johnson and Simpson (1985a). The experimental variation of the dye laser pulse width as a function of the pump pulse width (see Figure 10.20) was

$$t_{dye} \sim t_{pump}^{0.52}, \tag{25}$$

in excellent agreement with the square root dependence predicted by Ausschnitt and Jain (1978) and Ausschnitt et al. (1979).

Palfrey and Grischkowsky (1985) generated 16-fs frequency-tunable pulses by using a two-stage fiber pulse compressor together with an optical amplifier. Ishida and Yajima (1986) generated pulses of less than 100 fs tunable over 0.597 to 0.615 μm by taking the output from a cavity-dumped, hybridly mode-locked CW dye laser and coupling it to a single-stage fiber compressor. Damen and Shah (1988) reported on femtosecond luminescence spectroscopy of III-V semiconductors with 60-fs compressed pulses. The 60-fs pulses were derived from a compressed pulse-pumped synchronously mode-locked dye laser that was further compressed by a fiber-prism pulse compressor.

Applications of fiber-grating compressed pulses include picosecond photoconductive sampling characterization of semiconductor epitaxial films de-

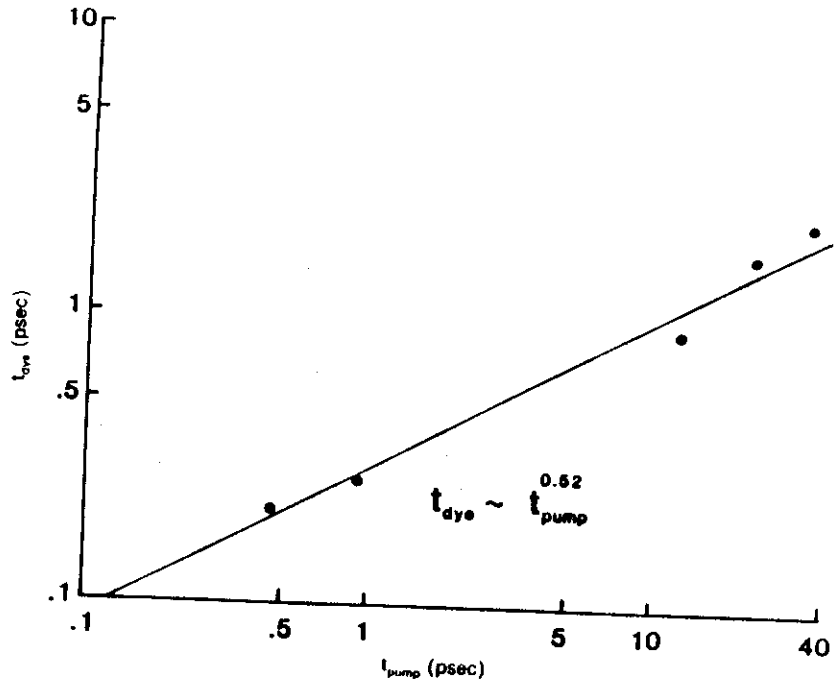

FIGURE 10.20. Temporal dynamics of the synchronous mode locking of the pellicle-tuned Rhodamine 6G dye laser as a function of the pump pulse duration, with the dye laser tuned to 0.595 μm.

posited on lattice-mismatched substrates (Johnson et al., 1985, 1987; Feldman et al., 1988), picosecond electro-optic sampling of GaAs integrated circuits (Kolner and Bloom, 1984, 1986; Weingarten et al., 1988), picosecond photoemission sampling of integrated circuits (Bokor et al., 1986; May et al., 1987, 1988) picosecond vacuum photodiode (Bokor et al., 1988), picosecond optical pulse shaping and spectral filtering (Dianov et al., 1985, 1986b; Haner and Warren, 1987; Heritage et al., 1985a, 1985b; Weiner et al., 1986), and the demonstration of an ultrafast light-controlled optical fiber modulator (Halas et al., 1987) and its use in the first experimental investigation of dark-soliton propagation in optical fibers (Krokel et al., 1988).

Recently, pulse compression techniques have been applied to the amplification of high-energy 1.06-μm pulses. The onset of self-focusing limits the amplification of ultrashort optical pulses. Fisher and Bischel (1974) proposed avoiding self-focusing in Nd:glass amplifiers by temporally broadening the input pulse to lower the pulse intensity. They noted that under certain circumstances, the glass nonlinearity would impress a chirp on the pulse that

Mourou (1985) and Maine et al. (1988) used an optical fiber to stretch a short optical pulse, amplify, and then recompress using a grating pair. Since the stretched pulse is amplified, the energy density can be increased, thereby more efficiently extracting the stored energy in the amplifier.

3. Femtosecond Pulse Compression

3.1 Theory

Remarkable progress has taken place in the compression of optical pulses. The theoretical limit in the visible spectrum is just a few femtoseconds. Already optical pulses as short as 6 fs have been generated and used in experiments (Fork et al., 1987; Brito Cruz et al., 1986). Such a pulse contains spectral components covering nearly the entire visible and near-infrared region of the spectrum. The short pulse itself is nearly an ideal continuum source.

It is useful to explore the limits of pulse compression in order to understand and appreciate the processes involved in compressing optical pulses in the femtosecond time regime. Attacking the limits provides a pathway for both utilizing and generating ever shorter optical pulses.

When an optical pulse propagates through any dielectric medium, group velocity dispersion broadens the pulse. For example, an 8-fs pulse will have its width doubled by passage through ~1 mm of glass or ~3 m of air. These linear propagation effects are not fundamental and can in principle be corrected by a linear compensation scheme.

One of the most useful pulse compressors, the grating-pair compressor devised by Treacy (1969) has been discussed earlier in this chapter. In his original paper, Treacy pointed out some of the limitations of this compressor for very short optical pulses having a large bandwidth. A grating pair induces a phase distortion on an optical pulse that becomes more severe as the ratio of the pulse bandwidth to the carrier frequency begins to approach unity.

The problem of generating ultrashort optical pulses reduces to minimizing the phase distortion. A useful way to discuss this problem is in terms of the Taylor series expansion of the phase:

$$\phi(\omega) = \phi(\omega_0) + \left(\frac{d\phi}{d\omega}\right)_{\omega_0}(\omega - \omega_0) + \frac{1}{2}\left(\frac{d^2\phi}{d\omega^2}\right)_{\omega_0}(\omega - \omega_0)^2 + \frac{1}{6}\left(\frac{d^3\phi}{d\omega^3}\right)_{\omega_0}(\omega - \omega_0)^3, \tag{26}$$

which is made around the central frequency, ω_0, of the pulse spectrum. Treacy has shown that a pair of diffraction gratings can be used to compensate for the quadratic phase distortion, $(d^2\phi/d\omega^2)_{\omega_0}$, of a frequency-broadened optical pulse. He pointed out in the same paper that the principal remaining problem in pulse compression of [illegible]

TABLE 10.2. Second and third derivatives of phase with respect to frequency for a double prism pair, a double grating pair, and material.

Prism	Grating	Material
$\frac{d^2\phi_p}{d\omega^2} = \frac{\lambda^3}{2\pi c^2}\frac{d^2P}{d\lambda^2}$	$\frac{d^2\phi_g}{d\omega^2} = \frac{\lambda^3 l_g}{\pi c^2 d^2}\left[1 - \left(\frac{\lambda}{d} - \sin\gamma\right)^2\right]^{-3/2}$	$\frac{d^2\phi_m}{d\omega^2} = \frac{\lambda^3 l_m}{2\pi c^2}\frac{d^2 n_m}{d\lambda^2}$
$\frac{d^3\phi_p}{d\omega^3} = \frac{\lambda^4}{4\pi^2 c^3}\left(3\frac{d^2P}{d\lambda^2} + \lambda\frac{d^3P}{d\lambda^3}\right)$	$\frac{d^3\phi_g}{d\omega^3} = \frac{-d^2\phi_g}{d\omega^2}\frac{6\pi\lambda}{c} \times \frac{\left(1 + \frac{\lambda}{d}\sin\gamma - \sin^2\gamma\right)}{\left[1 - \left(\frac{\lambda}{d} - \sin\gamma\right)^2\right]}$	$\frac{d^3\phi_m}{d\omega^3} = \frac{-\lambda^4 l_m}{4\pi^2 c^3}\left(3\frac{d^2 n_m}{d\lambda^2} + \lambda\frac{d^3 n_m}{d\lambda^3}\right)$

Derivatives of the path P in the prism sequence with respect to wavelength

$$\frac{d^2P}{d\lambda^2} = 4\left[\frac{d^2n}{d\lambda^2} + (2n - n^{-3})\left(\frac{dn}{d\lambda}\right)^2\right] l_p \sin\beta - 8\left(\frac{dn}{d\lambda}\right)^2 l_p \cos\beta$$

$$\frac{d^3P}{d\lambda^3} = 4\frac{d^3n}{d\lambda^3} l_p \sin\beta - 24\frac{dn}{d\lambda}\frac{d^2n}{d\lambda^2} l_p \cos\beta$$

TABLE 10.3. Second and third derivatives of phase with respect to frequency for the double prism pair and double grating pair described in the text.[a]

Derivative	Prisms	Gratings	Material
$\frac{d^2\phi}{d\omega^2}$ (fs^2)	$+648 - 32l_p$	$-3640 l_g$	$+2900 l_m$
$\frac{d^3\phi}{d\omega^3}$ (fs^3)	$+277 - 49l_p$	$+3120 l_g$	$+1620 l_m$

[a] Lengths are in centimeters.

uncompensated cubic phase distortion, $(d^3\phi/d\omega^3)_{\omega_0}$. Christov and Tomov (1986) also recognized this problem in a recent publication on optical fiber-grating compressors Tables 10.2 and 10.3 show phase derivatives for prisms and gratings.

To overcome the problem of unwanted cubic phase distortion an elegant solution has been devised. Both a grating pair and a prism pair induce a cubic phase distortion. We can take advantage of the fact that the cubic phase distortion for gratings and prisms is of the opposite sign by using a configuration where the compressed pulse is passed sequentially through a pair of gratings and a pair of prisms. In this manner it is possible to cancel the cubic phase distortion (Treacy, 1969).

The effect of a combination of prisms, gratings, and material on a pulse is [illegible]

$$\phi_T(\omega) = \phi_p(\omega) + \phi_g(\omega) + \phi_m(\omega), \tag{27}$$

where the subscripts p, g, and m refer to prisms, gratings, and material, respectively. The material of length l_m contributes a phase shift

$$\phi_m(\omega) = \frac{\omega l_m}{c} n_m(\omega), \tag{28}$$

where c is the speed of light and $n_m(\omega)$ the refractive index. For the prism-and-grating pair we follow the method described by Martinez et al. (1984). A grating pair in a double-pass configuration causes a phase shift

$$\phi_g(\omega) = \frac{2\omega l_g}{c}\left[1 - \left(\frac{2\pi c}{\omega d} - \sin\gamma\right)^2\right]^{1/2}, \tag{29}$$

where l_g is the grating spacing, d is the groove spacing, and γ is the angle of incidence.

For a double prism pair the phase shift is

$$\phi_p(\omega) = \frac{2\omega l_p}{c}\cos[\beta(\omega)], \tag{30}$$

where l_p is the distance between prism apices and $\beta(\omega)$ is the angle between the refracted ray at frequency ω and the line joining the two apices (Figure 10.21). For prisms with apex angle α and refractive index $n_p(\omega)$ the angle $\psi 2(\omega)$ at which the refracted ray leaves the first prism can be calculated by a straightforward application of Snell's law as a function of the angle of incidence ψ_1.

We define $\psi_{2\max}$ as the maximum angle at which a ray can leave the first prism and still intersect the apex of the second prism. Equation (30) can then be rewritten as

$$\phi_p(\omega) = \frac{2\omega l_p}{c}\cos[\psi_{2\max} - \psi_2(\omega)]. \tag{31}$$

Typical experimental values are $\alpha = 60°$, $\psi_1 = 47°$ (minimum deviation), $n_p(\omega_0) = 1.457$ (quartz prisms) at $\omega_0 = 3.1$ rad/fs ($\lambda_0 = 615$ nm), and $\psi_{2\max} = 49°$.

The total phase shift $\phi_T(\omega)$ can be calculated numerically for conditions typical of recent ultrashort-pulse-compression experiments by using Eqs. (28), (29), and (31) to provide a group delay dispersion $d^2\phi_T/d\omega^2|_{\omega_0}$ of -700 fs^2 and to cause the derivative of the group delay dispersion, $d^3\phi_T/d\omega^3$, to be zero at the center frequency of the pulse. The value of $d^2\phi_T/d\omega^2$ is such as to compensate the linear frequency sweep generated on a 60-fs, 200-kW pulse propagated through a 0.9-cm quartz fiber with a 4-μm core diameter. The prism spacing, grating spacing, and material length used in the numerical calculations are $l_p = 74$ cm, $l_g = 0.7$ cm, and $l_m = 0.5$ cm of quartz, respectively. The angle of incidence at the first grating was 45°, and the number of grooves per millimeter was 600.

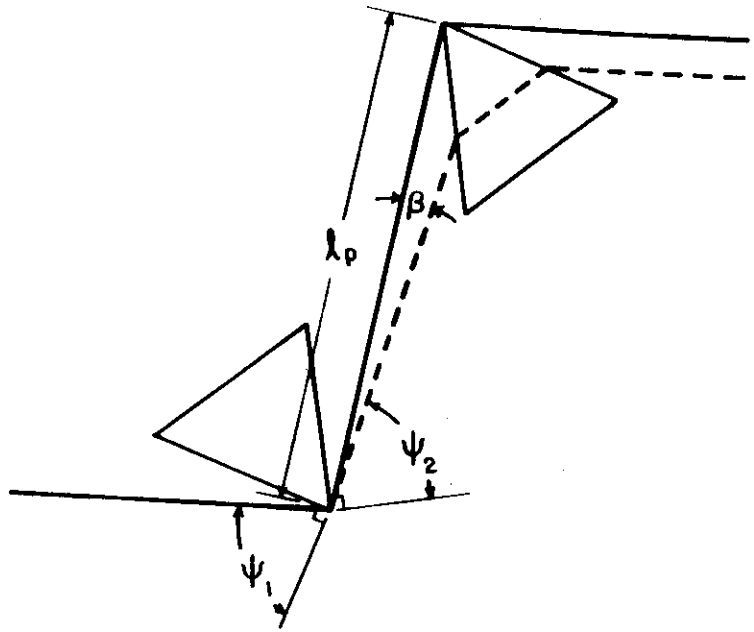

FIGURE 10.21. Parameters used in describing propagation of the optical pulse through the prism sequence. The angle of incidence at the face of the first prism is ψ_1 and the angle with respect to the normal to the exit face is ψ_2. The angle between a line drawn between prism apices and the direction of a ray exiting the first prism at ψ_2 is denoted by β. The distance between prism apices is l_p.

The departure of this compressor based on prisms and gratings from an ideal quadratic compressor can be evaluated by examining the variation of the group delay dispersion, $d^2\phi_T(\omega)/d\omega^2$, with frequency (Figure 10.22). One sees that this combination of prisms, gratings, and material provides the value of group delay dispersion required to compensate for the linear chirp in the pulse. At the same time, this combination of prisms, gratings, and material makes the derivative of the group delay dispersion zero at the center frequency of the pulse. This minimizes the cubic distortion and leaves as the main contribution to the phase that which is due to the curvature of the group delay dispersion ($d^4\phi/d\omega^4 \neq 0$) across the spectral range of the pulse.

The consequence of the departure of these actual compressors from an ideal quadratic compressor can be examined by calculating the temporal profile of the compressed pulse given a hypothetical incident pulse with an ideal quadratic phase distortion. In particular, we compare a compressor using prisms and gratings with a compressor using the gratings alone. Figure 10.23 shows the calculated intensity profile for the case when prisms, gratings, and material are used with the same parameters as in Figure 10.22. The

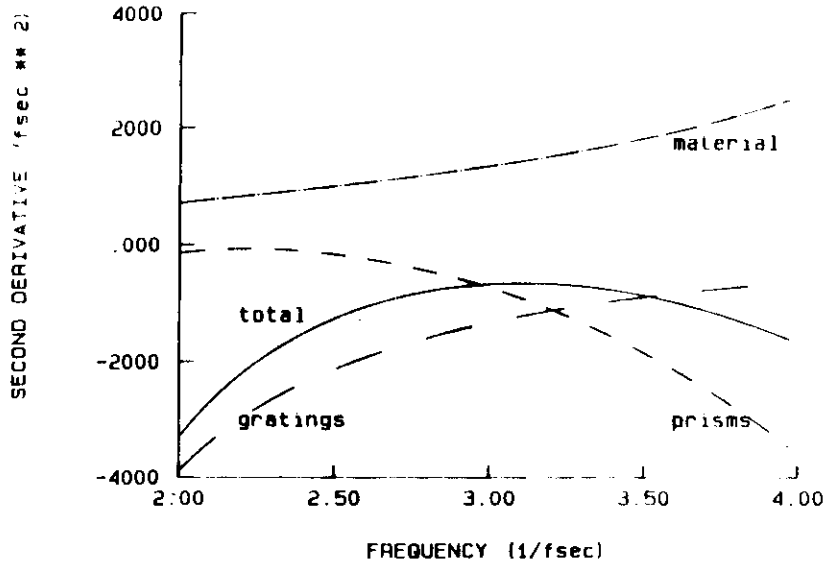

FIGURE 10.22. Plot of the second derivative of phase with respect to frequency for the prisms (short dash), gratings (long dash), and material (dash-dot) and for the total phase shift (solid).

of the incoming pulse was chosen to be 0.5 rad/fs, which corresponds to a transform-limited pulse duration of 4 fs. In both Figures 10.23a and 10.23b the linear frequency sweep has been compensated for, but only in the case of the compressor with prism pair, grating pair, and dispersive material (Figure 10.23b) was it possible to compensate for the parabolic frequency sweep by setting the cubic phase distortion to zero.

The oscillatory trailing edge on the pulse shown in Figure 10.23a is due to the uncompensated cubic distortion, which causes the high- and low-frequency edges of the pulse spectrum to lag with respect to the center frequency. These delayed frequency components beat with each other to create an oscillatory trailing edge on the pulse. If prisms are used alone, the compressed pulse is similar to that shown in Figure 10.23a but with the time axis reversed; that is, the oscillatory trailing edge becomes an oscillatory leading edge.

The dominant residual distortion of the phase-corrected pulse is that which is due to the uncorrected negative curvature of the group velocity dispersion $d^4\phi/d\omega^4 < 0$. The effect is to leave small oscillatory wings on the leading and trailing edges of the pulse, as is evident from Figure 10.23b, and to broaden the main peak slightly. The lower limit on the duration of pulses compressed in this manner depends on the specific shape of the input-pulse spectrum and

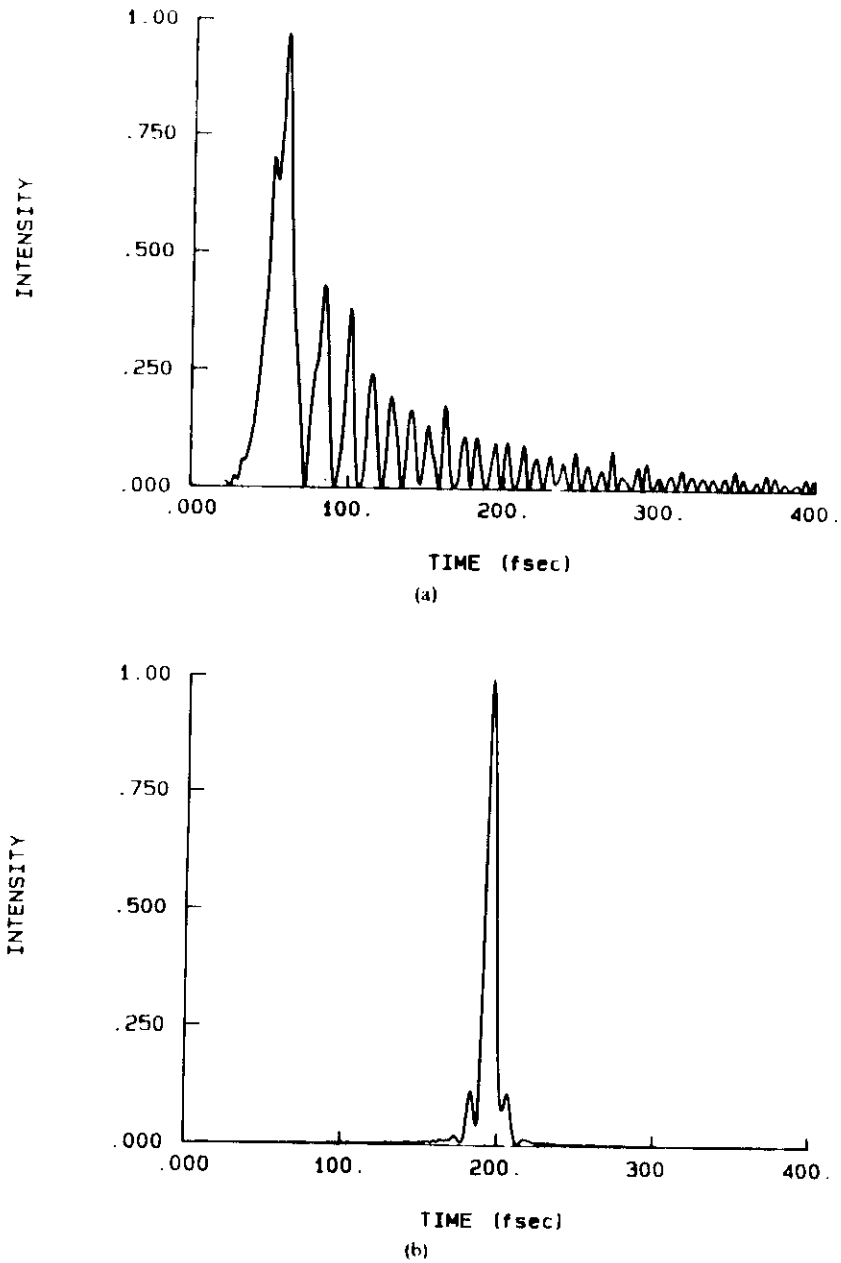

FIGURE 10.23. Calculated pulse intensity vs. time for the case of compression using only gratings and material dispersion (a) and for the case of compression using a combination of prisms, gratings, and material dispersion (b).

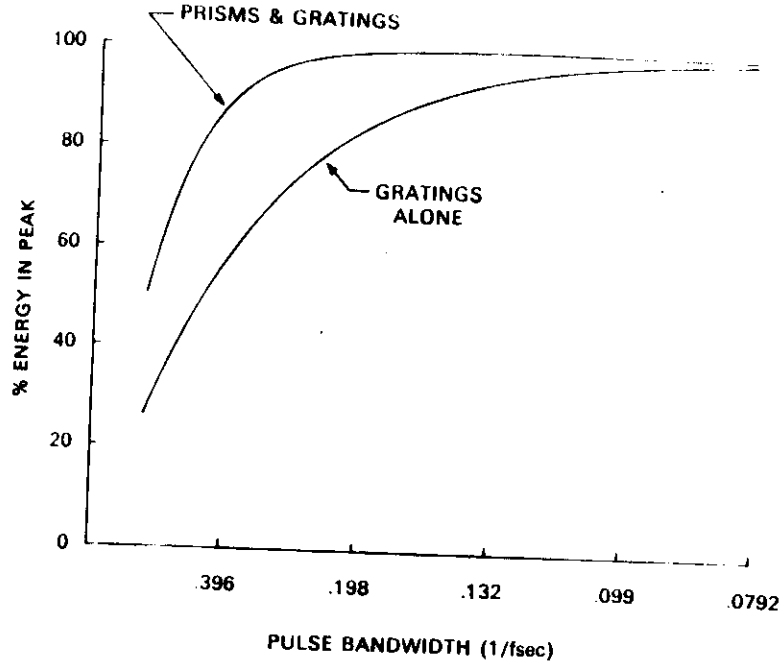

FIGURE 10.24. Plot of energy in the main peak of the compressed pulse for the case of combined prisms and gratings and for the case of gratings alone.

assumed above, the minimum compressed pulse width is between 6 and 7 fs, which is in approximate agreement with recently observed pulses compressed with grating and prism pairs (Fork et al., 1987). In Figure 10.24 the energy in the pulse peak is plotted versus pulse bandwidth for the case of gratings alone and the grating-prism pair combination.

3.2 Experiment

The arrangement of gratings and prisms for pulse compression is illustrated in Figure 10.25. The experimental study was carried out using optical pulses generated in a colliding-pulse mode-locked laser that contained an intracavity prism sequence identical to the four-prism set shown in Figure 10.25. These pulses were amplified at a repetition rate of 8 kHz in a copper-vapor laser-pumped amplifier to energies of $\sim 1\ \mu J$. The amplified pulses had durations of 50 fs and a spectrum centered at 620 nm. A fraction of the amplified pulse energy was coupled into a polarization-preserving quartz fiber with core dimensions of $\sim 4\ \mu m$ and a length of 0.9 cm. The optical intensity in the fiber was $1\ 2 \times 10^{12}$ W/cm.

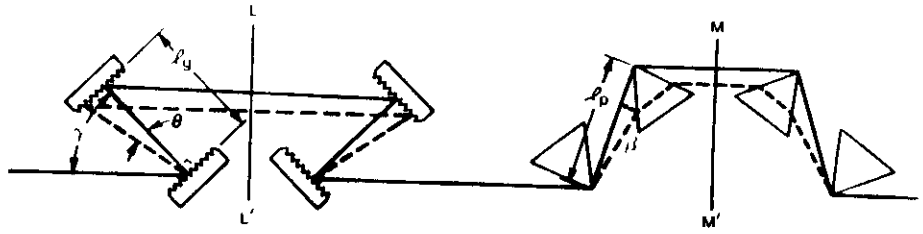

FIGURE 10.25. Combined grating and prism sequence used to remove both quadratic and cubic phase distortion. The solid line is a reference line. The dashed line is the path of a plane wave that propagates between the gratings at an angle θ with respect to the normal to the grating faces and between the prism pairs at an angle β with respect to a line drawn between the prism apices. The plane LL' is a plane of symmetry for the grating sequence, and the plane MM' is a plane of symmetry for the prism sequence.

A four-prism sequence was then introduced, so the combined prism and grating sequence was equivalent to that shown in Figure 10.25. It was then possible to adjust the spacing of the prism and grating pairs so the maxima of the six different upconverted intensity traces all occurred at the same phase delay. Subsequent optimization was done by monitoring the interferometric autocorrelation (Diels et al., 1978, 1985) trace of the compressed pulse while adjusting the prism spacing l_p and the grating spacing l_g. It is not possible to use the more conventional background-free autocorrelation technique for pulses this short since even a small relative angle between wave vectors of the interacting beams introduces measurable error. It was also necessary to use an extremely thin (32-μm) KDP crystal to double the compressed pulse so as to minimize distortion by group velocity dispersion within the doubling crystal.

The interferometric autocorrelation trace obtained on optimizing l_p and l_g is shown in Figure 10.26. The prism spacing for this trace was $l_p = 71$ cm, and the grating spacing was $l_g = 0.5$ cm. For purposes of comparison we have used crosses to indicate the calculated maxima and minima for an interferometric autocorrelation trace of a hyperbolic-secant-squared pulse having zero phase distortion and a full width at half-maximum of 6 fs. The close fit between the calculated and experimental interferometric autocorrelation functions indicates an absence of significant phase distortion over the bandwidth of the pulse. The well-resolved interference maxima also provide a rigorous calibration of the relative delay.

3.3 Applications

The success in generating optical pulses as short as 6 fs opens up the domain of physical processes that take place in a few femtosecond

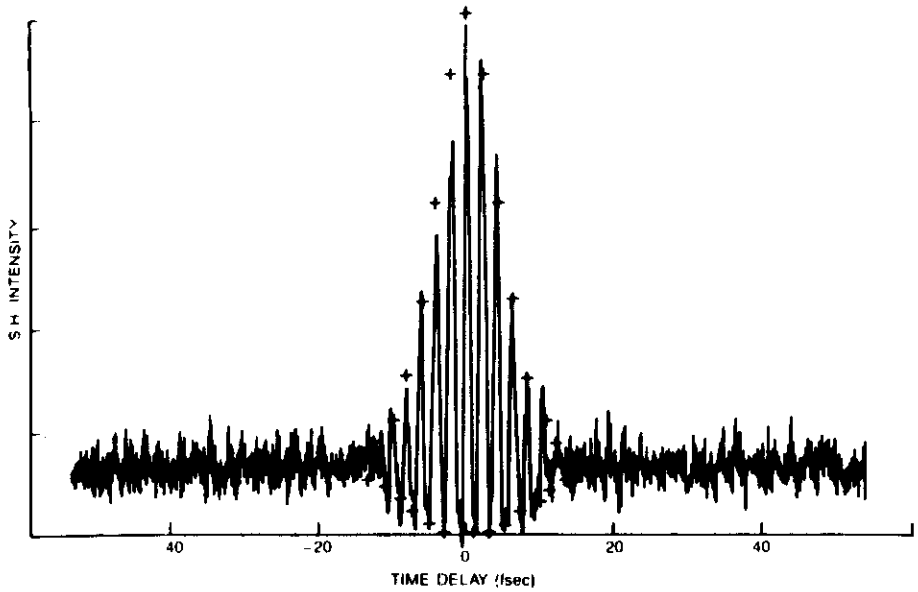

FIGURE 10.26. Experimental interferometric autocorrelation trace for a compressed pulse for $l_p = 71$ cm and $l_g = 0.5$ cm. The interference maxima and minima calculated for the interferometric autocorrelation trace for a hyperbolic-secant-squared pulse of 6-fs duration are indicated by crosses. The close agreement between experiment and theory demonstrates absence of significant phase distortion in the compressed pulse.

that is so short contains frequency components from almost the entire visible region of the spectrum. Such a pulse is a nearly ideal continuum source. The well-defined temporal and spectral character of the pulse makes it quite useful for time-resolved spectroscopic problems.

Ultrashort optical pulse techniques provide a unique means for investigating nonequilibrium energy redistribution among vibronic levels in large organic molecules in solution. Previously, the dynamics of induced absorbance changes have been measured using pump and probe pulses having the same frequency spectrum. In the experiments described here induced absorption changes of optically excited molecules over a broad spectral range of 2400 cm^{-1} centered at the energy of the excitation pulse were measured while maintaining a 10-fs time resolution. These experiments permit the observation of time-resolved hole burning and the process of equilibration to a thermalized population distribution on a femtosecond time scale (Brito Cruz et al., 1986, 1988b).

The absorption spectrum of a large dye molecule is dominated by vibronic transitions from a thermalized group state. Typically, these large molecules, which have a molecular weight of 400 or more, have a large number of degrees of freedom. The optical absorption coefficient may be written as a sum over

transitions from occupied vibrational levels in the ground state to vibrational levels in the excited state. The absorption coefficient is given by

$$\alpha(\nu) = C \sum_{ij} P_i M^2 \chi_{ij} \nu g(\nu - \nu_{ij}), \tag{7}$$

where C is a constant, P_i is the thermal occupation probability of the initial state, M is the dipole moment of the electronic transition, χ_{ij} is the Franck-Condon factor, and g is the line shape profile for each transition. The above expression describes the molecular system in thermal equilibrium. With a short optical pulse it is possible to excite a band of states that are resonant with the pumping energy. Before the molecular system comes into equilibrium, bleaching is observed in a spectral range determined by the convolution of the pump spectrum with the line shape profile of the individual transitions. As time progresses, the system relaxes to thermal equilibrium due to interaction with the thermal bath. The thermal bath couples to the vibronic levels by both intramolecular and intermolecular processes. The large number of degrees of freedom in the molecular backbone can form a thermal bath within the molecule itself. It is also possible for intermolecular energy transfer to take place on a somewhat longer time scale by collisions, dipole-dipole interaction, etc.

The experimental apparatus is arranged to perform a pump-probe type of experiment with one important modification over previous experiments. The probe pulse is approximately 10 fs in duration and has a significantly broader bandwidth than the 60-fs pump pulse. The pumping and probing pulses are derived from the same initial amplified 60-fs optical pulse having an energy of 1 μJ with a center frequency at 618 nm. The probe pulse is formed by passing a portion of the initial pulse through a 12-nm length of optical fiber followed by a grating-pair compressor. The shorter pulse is then used to probe the absorption spectrum by passing through the excited sample into a spectrometer and diode array. Care is taken to compensate for group velocity dispersion in the probe optical path. The experiments are performed at a repetition rate of 8 kHz.

The dyes are dissolved in ethylene glycol at concentrations that yield optical attenuations of less than $1/e$ when the dye solution is flowed through a jet with a thickness of 100 to 300 μm. The pump pulses are attenuated to levels that induce absorption changes of a few percent or less.

The data are collected by a differential measuring technique. The pump beam is periodically blocked by a shutter at a frequency of 10 Hz and the transmitted spectra are recorded in the computer memory in phase with the chopped pumping beam. Spectra are recorded at different time delays as determined by the optical path delay, which is controlled by a stepping motor translation stage. Integration time for a single spectrum is typically 30 s.

In Figure 10.27 the absorption spectrum for cresyl violet is plotted before and after excitation with a 60-fs optical pulse at 618 nm for zero relative time delay. A decrease in absorption is clearly observed in the spectral region close

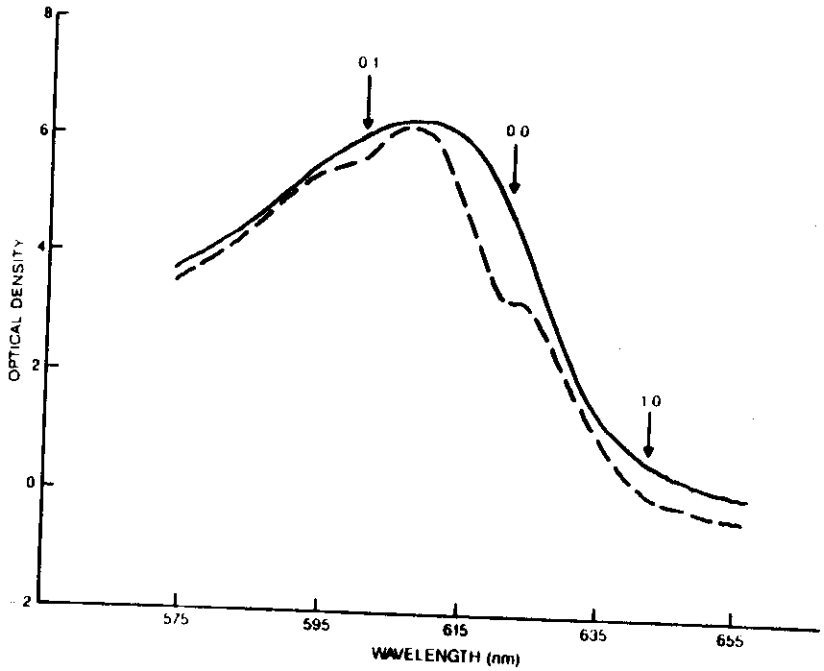

FIGURE 10.27. Plot of the absorbance spectrum of the molecule cresyl violet near zero time delay before (solid line) and after (dashed line) excitation with a 60-fs optical pulse.

to the pumping wavelength. In addition, replica holes are seen approximately 600 cm^{-1} above and below the excitation energy. In Figure 10.28 the time-resolved differential spectra are plotted for cresyl violet. The time delay between spectra is 25 fs. The central hole and the two adjacent replica holes are seen to broaden and form a thermalized spectrum in the first few hundred femtoseconds following excitation.

The mechanism for the formation of the replica holes is readily understood. Measurements of the Raman spectra of cresyl violet reveal the presence of a strong mode at 590 cm^{-1}. In a large molecule with a large number of degrees of freedom a correspondingly large number of modes can contribute to the absorption spectrum, as illustrated with Figure 10.27. Usually only a few modes with energies larger than kT change their occupation number during the optical transition to the excited state. These modes are called active or system modes and have large Franck-Condon factors. The strength of the absorption is determined by the Franck-Condon factor χ_{if}. The 598-cm^{-1} mode appears to be the dominant mode in the absorption spectrum as evidenced by bleaching both at the 0–0 transition, which is at the excitation energy, and at the 0–1 and 1–0 positions of the Franck-Condon progression.

The relative strengths of the bleaching at the central hole and at the replica

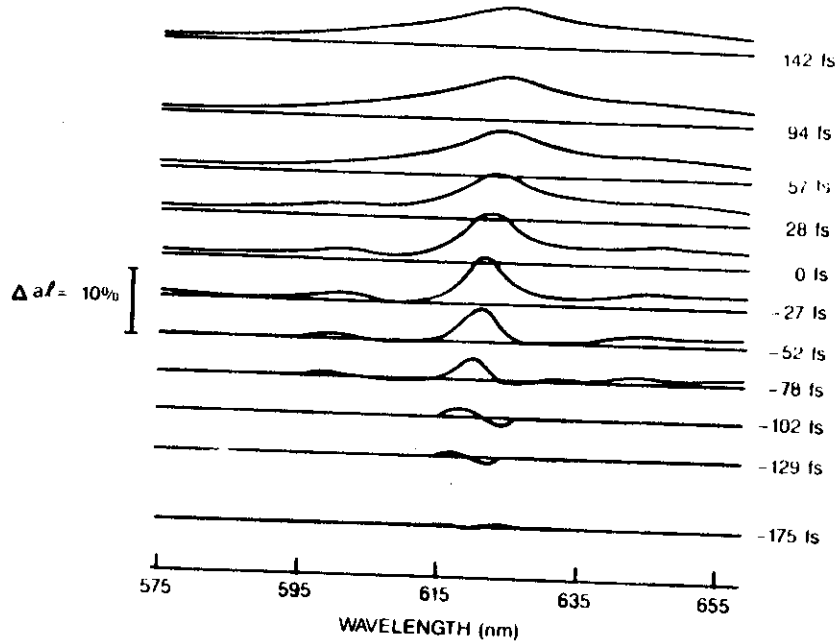

FIGURE 10.28. Differential absorbance spectra plotted as a function of relative time delay following excitation with a 60-fs optical pulse at 618 nm for the molecule cresyl violet.

holes can be determined by estimating the Franck-Condon factors in the harmonic approximation. We calculate $\chi_{00}/\chi_{01,10} = 0.26$, which is consistent with the experimental observation value.

The hole observed in Figure 10.28 broadens and relaxes to the quasi-equilibrium spectrum within the first few hundred femtoseconds. If we assume that the inhomogeneous linewidth is much larger than the homogeneous linewidth, we can estimate the polarization dephasing time T_2 from the width of the hole burned in the spectrum. For the case of a Lorentzian profile, where $\Delta\lambda$ is the half-width of the hole, the expression for T_2 is given by $T_2 = 2\lambda^2/\pi c\Delta\lambda$. Using the above expression we determine T_2 to be 75 fs for cresyl violet.

Some insight into the energy relaxation of the excited molecules can be obtained by looking at the time evolution of the differential absorption at different spectral regions within our range of observation. In Figure 10.29 we plot this evolution for a region 7 nm wide around 587, 625, and 654 nm. The curve for 625 nm shows the evolution of the population in levels that are very close in energy to the levels excited by the pump. In this spectral region an overshoot in the bleaching occurs as a

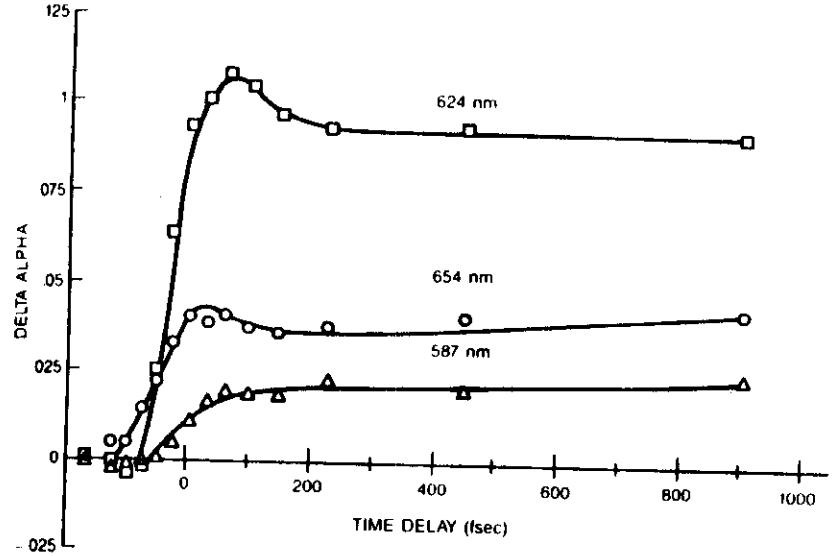

FIGURE 10.29. Plot of the differential absorption spectrum in time for three selected wavelengths for the molecule cresyl violet. (The lines are to guide the eye.)

burning and a rapid recovery on the order of 50 fs is observed as the ground and excited states become thermalized. The bleaching at 654 nm also shows a small overshoot, which recovers as the nonequilibrium distribution transits to a thermalized distribution in the first few hundred picoseconds. On the high-energy side at 587 nm a slower rise is observed as the molecular distribution thermalizes.

References

Agostinelli, J., G. Harvey, T. Stone, and C. Gabel (1979) Appl. Opt. **18**, 2500.
Alfano, R.R. and P.P. Ho (1988) IEEE J. Quantum Electron.**QE-24**, 351.
Alfano, R.R. and S.L. Shapiro (1970) Phys. Rev. Lett. **24**, 592.
Arthurs, E.G., D.J. Bradley, and A.G. Roddie (1971) Appl. Phys. Lett. **19**, 480.
Ausschnitt, C.P. and R.K. Jain (1978) Appl. Phys. Lett. **32**, 727.
Ausschnitt, C.P., R.K. Jain, and J.P. Heritage (1979) IEEE J. Quantum Electron. **QE-15**, 912.
Auyeung, J. and A. Yariv (1978) IEEE J. Quantum Electron. **QE-14**, 347.
Baldeck, P.L., F. Raccah, and R.R. Alfano (1987) Opt. Lett. **12**, 588.
Beaud, P., B. Zysset, A.P. Schwarzenbach, and H.P. Weber (1986) Opt. Lett. **11**, 24.
Bloembergen, N. and P. Lallemand (1966) Phys. Rev. Lett. **16**, 81.
Blow, K.J., N.J. Doran, and B.P. Nelson (1985) Opt. Lett. **10**, 393.
Bokor, J., A.M. Johnson, R.H. Storz, and W.M. Simpson (1986) Appl. Phys. Lett. **49**, 226.

Bokor, J., A.M. Johnson, W.M. Simpson, R.H. Storz, and P.R. Smith (1988) Appl. Phys. Lett. **53**, 2599.
Bondarenko, N.G., I.V. Eremina, and V.I. Talanov (1970) JETP Lett. **12**, 85.
Bor, Z. and B. Racz (1985) Opt. Commun. **54**, 165.
Bourkoff, E., W. Zhao, R.I. Joseph, and D.N. Christodoulides (1987a) Opt. Lett. **12**, 272.
Bourkoff, E., W. Zhao, R.I. Joseph, and D.N. Christodoulides (1987b) Opt. Commun. **62**, 284.
Bradley, D.J., G.H.C. New, and S.J. Caughey (1970) Phys. Lett. **32A**, 313.
Brewer, R.G. (1967) Phys. Rev. Lett. **19**, 8.
Brito Cruz, C.H., R.L. Fork, W.H. Knox, and C.V. Shank (1986) Chem. Phys. Lett. **132**, 341.
Brito Cruz, C.H., P.C. Becker, R.L. Fork, and C.V. Shank (1988a) Opt. Lett. **13**, 123.
Brito Cruz, C.H., J.P. Gordon, P.C. Becker, R.L. Fork, C.V. Shank (1988b) IEEE J. Quantum Electron. **24**, 261.
Butylkin, V.S., V.V. Grigoryants, and V.I. Smirnov (1979) Opt. Quantum Electron. **11**, 141.
Christov, I.P. and I.V. Tomov (1986) Opt. Commun. **58**, 338.
Damen, T.C., and J. Shah (1988) Appl. Phys. Lett. **52**, 1291.
Damm, T., M. Kaschke, F. Noack, and B. Wilhelmi (1985) Opt. Lett. **10**, 176.
DeMartini, F., C.H. Townes, T.K. Gustafson, and P.L. Kelley (1967) Phys. Rev. **164**, 312.
Desbois, J., F. Gires, and P. Tournois (1973) IEEE J. Quantum Electron. **QE-9**, 213.
Dianov, E.M., A. Ya. Karasik, P.V. Mamyshev, G.I. Onishchukov, A.M. Prokhorov, M.F. Stel'makh, and A.A. Fomichev (1984a) Sov. J. Quantum Electron. **14**, 726.
Dianov, E.M., A.Y. Karasik, P.V. Mamyshev, G.I. Onishchukov, A.M. Prokhorov, M.F. Stel'makh, and A.A. Fomichev (1984b). JETP Lett. **39**, 691.
Dianov, E.M., A.Y. Karasik, P.G. Mamyshev, A.M. Prokhorov, and V.N. Serkin (1985) Sov. Phys. JETP **62**, 448.
Dianov, E.M., L.M. Ivanov, A.Y. Karasik, P.V. Mamyshev, and A.M. Prokhorov (1986a) Sov. Phys. JETP **64**, 1205.
Dianov, E.M., L.M. Ivanov, A.Y. Karasik, P.V. Mamyshev, and A.M. Prokhorov (1986b) JETP Lett. **44**, 156.
Dianov, E.M., A.Y. Karasik, P.V. Mamyshev, A.M. Prokhorov, and D.G. Fursa (1987) Sov. J. Quantum Electron. **17**, 415.
Dianov, E.M., P.V. Mamyshev, and A.M. Prokhorov (1988) Sov. J. Quantum Electron. **18**, 1.
Diels, J.-C., E.W. Stryland and D. Gold (1978) In *Proceedings of the First International Conference on Picosecond Phenomena*, p. 117. Springer-Verlag, Berlin.
Diels, J.-C., J.J. Fontaine, I.C. McMichael, and F. Simoni (1985) Appl. Opt. **24**, 1270.
Duguay, M.A. (1976) The ultrafast optical Kerr shutter. In *Progress in Optics XII*, E. Wolf, ed., p. 161. North-Holland, Amsterdam.
Duguay, M.A. and J.W. Hansen (1969) Appl. Phys. Lett. **14**, 14.
Dupuy, C.G. and P. Bado (1984) Dig. Conf. Lasers and Electro-Opt., Anaheim, Calif., paper TUE2, 58.
Feldman, R.D., R.F. Austin, P.M. Bridenbaugh, A.M. Johnson, W.M. Simpson, B.A. Wilson, and C.E. Bonner (1988) J. Appl. Phys. **64**, 1191.
Fisher, R.A. and W.K. Bischel (1974) Appl. Phys. Lett. **24**, 468.

Fisher, R.A., P.L. Kelley, and T.K. Gustafson (1969) Appl. Phys. Lett. **14**, 140.
Fork, R.L., O.E. Martinez, and J.P. Gordon (1984) Opt. Lett. **9**, 150.
Fork, R.L., C.H. Brito Cruz, P.C. Becker, and C.V. Shank (1987) Opt. Lett. **12**, 483.
Fujimoto, J.G., A.M. Weiner, and E.P. Ippen (1984) Appl. Phys. Lett. **44**, 832.
Giordmaine, J.A., M.A. Duguay, and J.W. Hansen (1968) IEEE J. Quantum Electron. **QE-4**, 252.
Gires, F. and P. Tournois (1964) C.R. Acad. Sci. (Paris) **258**, 6112.
Gloge, D. (1971) Appl. Opt. **10**, 2252.
Golovchenko, E.A., E.M. Dianov, P.V. Mamyshev, and A.M. Prokhorov (1988) Opt. Quantum Electron. **20**, 343.
Gomes, A.S., U. Osterberg, W. Sibbett, and J.R. Taylor (1985a) Opt. Commun. **54**, 377.
Gomes, A.S., W. Sibbett, and J.R. Taylor (1985b) Opt. Lett. **10**, 338.
Gomes, A.S., W. Sibbett, and J.R. Taylor (1985c) IEEE J. Quantum Electron. **QE-21**, 1157.
Gomes, A.S.L., W. Sibbett, and J.R. Taylor (1986a) Appl. Phys. B **39**, 43.
Gomes, A.S.L., W.E. Sleat, W. Sibbett, and J.R. Taylor (1986b) Opt. Commun. **57**, 257.
Gomes, A.S.L., V.L. da Silva, and J.R. Taylor (1988a) J. Opt. Soc. Am. B **5**, 373.
Gomes, A.S.L., A.S. Gouveia-Neto, and J.R. Taylor (1988b) Opt. Quantum Electron. **20**, 95.
Grischkowsky, D. and A.C. Balant (1982a) Appl. Phys. Lett. **41**, 1.
Grischkowsky, D. and Balant, A.C. (1982b) Optical pulse compression with reduced wings. In *Picosecond Phenomena III*, K.B. Eisenthal, R.M. Hochstrasser, W. Kaiser, and A. Laubereau, eds., p. 123. Springer-Verlag, Berlin.
Gustafson, T.K., J.P. Taran, H.A. Haus, J.R. Lifsitz, and P.L. Kelley (1969) Phys. Rev. **177**, 306.
Halas, N.J., D. Krokel, and D. Grischkowsky (1987) Appl. Phys. Lett. **50**, 886.
Halbout, J.-M. and D. Grischkowsky (1984) Appl. Phys. Lett. **45**, 1281.
Haner, M. and W.S. Warren (1987) Opt. Lett. **12**, 398.
Heritage, J.P., R.N. Thurston, W.J. Tomlinson, A.M. Weiner, and R.H. Stolen (1984) J. Opt. Soc. Am. A **1**, 1288A.
Heritage, J.P., R.N. Thurston, W.J. Tomlinson, A.M. Weiner, and R.H. Stolen (1985a) Appl. Phys. Lett. **47**, 87.
Heritage, J.P., A.M. Weiner, and R.N. Thurston (1985b) Opt. Lett. **10**, 609.
Heritage, J.P., A.M. Weiner, R.J. Hawkins, and O.E. Martinez (1988) Opt. Commun. **67**, 367.
Hian-Hua, L., L. Yu-Lin, and J. Jia-Lin (1985) Opt. Quantum Electron. **17**, 187.
Ippen, E.P. and C.V. Shank (1975a) Appl. Phys. Lett. **26**, 92.
Ippen, E.P. and C.V. Shank (1975b) Appl. Phys. Lett. **27**, 488.
Ippen, E.P., C.V. Shank, and T.K. Gustafson (1974) Appl. Phys. Lett. **24**, 190.
Ishida, Y. and T. Yajima (1986) Opt. Commun. **58**, 355.
Iwashita, K., K. Nakagawa, Y. Nakano, and Y. Suzuki (1982) Electron. Lett. **18**, 873.
Johnson, A.M. and W.M. Simpson (1983) Opt. Lett. **8**, 554.
Johnson, A.M. and W.M. Simpson (1985a) J. Opt. Soc. Am. B **2**, 619.
Johnson, A.M. and W.M. Simpson (1985b) Proc. SPIE **533**, 52.
Johnson, A.M. and W.M. Simpson (1986) IEEE J. Quantum Electron. **QE-22**, 133.
Johnson, A.M., R.H. Stolen, and W.M. Simpson (1984a) Appl. Phys. Lett. **44**, 729.
Johnson, A.M., R.H. Stolen, and W.M. Simpson (1984b) Generation of 0.41-picosecond pulses by the single-state compression of frequency doubled Nd:YAG laser pulses. In *Ultrafast Phenomena IV*, D.H. Auston and K.B. Eisenthal, eds., p. 16. Springer-Verlag, Berlin.
Johnson, A.M., D.W. Kisker, W.M. Simpson, and R.D. Feldman (1985) Picosecond photoconductivity in polycrystalline CdTe films prepared by UV-enhanced OMCVD. In *Picosecond Electronics and Optoelectronics*, G.A. Mourou, D.M. Bloom, and C.-H. Lee, eds., p. 188. Springer-Verlag, Berlin.
Johnson, A.M., R.H. Stolen, and W.M. Simpson (1986) The observation of chirped stimulated Raman scattered light in fibers. In *Ultrafast Phenomena V*, G.R. Fleming and A.E. Siegman, eds., p. 160. Springer-Verlag, Berlin.
Johnson, A.M., R.M. Lum, W.M. Simpson, and J. Klingert (1987) IEEE J. Quantum Electron. **QE-23**, 1180.
Kafka, J.D. and T. Baer (1985) Proc. SPIE **533**, 38.
Kafka, J.D. and T. Baer (1986) Proc. SPIE **610**, 2.
Kafka, J.D. and T. Baer (1987) Opt. Lett. **12**, 401.
Kafka, J.D. and T.M. Baer (1988) IEEE J. Quantum Electron. **QE-24**, 341.
Kafka, J.D., B.H. Kolner, T. Baer, and D.M. Bloom (1984) Opt. Lett. **9**, 505.
Keller, U., J.A. Valdmanis, M.C. Nuss, and A.M. Johnson (1988) IEEE J. Quantum Electron. **QE-24**, 427.
Klauder, J.R., A.C. Price, S. Darlington, and W.J. Albersheim (1960) Bell System Tech. J. **39**, 745.
Knox, W.H., R.L. Fork, M.C. Downer, R.H. Stolen, C.V. Shank, and J.A. Valdmanis (1985) Appl. Phys. Lett. **46**, 1120.
Kolner, B.H. and D.M. Bloom (1984) Electron. Lett. **20**, 818.
Kolner, B.H. and D.M. Bloom (1986) IEEE J. Quantum Electron. **QE-22**, 79.
Krokel, D., N.J. Halas, G. Giulinai, and D. Grishckowsky (1988) Phys. Rev. Lett. **60**, 29.
Kuckartz, M., R. Schulz, and H. Harde (1987) Opt. Quantum Electron. **19**, 237.
Kuckartz, M., R. Schulz, and H. Harde (1988) J. Opt. Soc. Am. B **5**, 1353.
Lassen, H.E., F. Mengel, B. Tromborg, N.C. Albertsen, and P.L. Christiansen (1985) Opt. Lett. **10**, 34.
Laubereau, A. (1969) Phys. Lett. **29A**, 539.
Lehmberg, R.H. and J.M. McMahon (1976) Appl. Phys. Lett. **28**, 204.
Lin, C., L.G. Cohen, R.H. Stolen, G.W. Tasker, and W.G. French (1977) Opt. Commun. **20**, 426.
Maine, P., D. Strickland, P. Bado, M. Pessot, and G. Mourou (1988) IEEE J. Quantum Electron. **24**, 398.
Martinez, O.E., J.P. Gordon, and R.L. Fork (1984) J. Opt. Soc. Am. A **1**, 1003.
May, P., J.-M. Halbout, and G. Chiu (1987) Appl. Phys. Lett. **51**, 145.
May, P., J.-M. Halbout, and G. Chiu (1988) IEEE J. Quantum Electron. **QE-24**, 234.
Meinel, R. (1983) Opt. Commun. **47**, 343.
Mollenauer, L.F. (1985) Philos. Trans. R. Soc. London A **315**, 437.
Mollenauer, L.F. and R.H. Stolen (1982) Laser Focus **18(4)**, 193.
Mollenauer, L.F., R.H. Stolen, and J.P. Gordon (1980) Phys. Rev. Lett. **45**, 1095.
Mollenauer, L.F., R.H. Stolen, J.P. Gordon, and W.J. Tomlinson (1983) Opt. Lett. **8**, 289.
Mollenauer, L.F., J.P. Gordon, and M.N. Islam (1986) IEEE J. Quantum Electron. **QE-22**, 157.
Nakashima, T., M. Nakazawa, K. Nishi, and H. Kubota (1987) Opt. Lett. **12**, 404.
Nakatsuka, H. and D. Grischkowsky (1981) Opt. Lett. **6**, 13.

Nakatsuka, H., D. Grischkowsky, and A.C. Balant (1981) Phys. Rev. Lett. **47**, 910.
Nakazawa, M., T. Nakashima, and H. Kubota (1988) Opt. Lett. **13**, 120.
Nikolaus, B. and D. Grischkowsky (1983a) Appl. Phys. Lett. **42**, 1.
Nikolaus, B. and D. Grischkowsky (1983b) Appl. Phys. Lett. **43**, 228.
Ohmori, Y., Y. Sasaki, and T. Edahiro (1983) Trans. IECE Jpn. **E-66**, 146.
Owyoung, A., R.W. Hellwarth, and N. George (1972) Phys. Rev. B **5**, 628.
Palfrey, S.L. and D. Grischkowsky (1985) Opt. Lett. **10**, 562.
Payne, D.N. and W.A. Gambling (1975) Electron. Lett. **11**, 176.
Roskos, H., A. Seilmeier, W. Kaiser, J.D. Harvey (1987) Opt. Commun. **61**, 81.
Rothenberg, J.E. and D. Grischkowsky (1989) Phys. Rev. Lett. **62**, 531.
Schadt, D. and B. Jaskorzynska (1987) J. Opt. Soc. Am. B **4**, 856.
Schadt, D., B. Jaskorzynska, and U. Österberg (1986) J. Opt. Soc. Am. B **3**, 1257.
Shank, C.V., R.L. Fork, R. Yen, R.H. Stolen, and W.J. Tomlinson (1982) Appl. Phys. Lett. **40**, 761.
Shapiro, S.L. and H.P. Broida (1967) Phys. Rev. **154**, 129.
Shimizu, F. (1967) Phys. Rev. Lett. **19**, 1097.
Smith, R.G. (1972) Appl. Opt. **11**, 2489.
Stolen, R.H. (1979a) IEEE J. Quantum Electron. **QE-15**, 1157.
Stolen, R.H. (1979b) Nonlinear properties of optical fibers. In *Optical Fiber Telecommunications*, S.E. Miller and A.G. Chynoweth eds., chapter 5. Academic Press, New York.
Stolen, R.H. and E.P. Ippen (1973) Appl. Phys. Lett. **22**, 276.
Stolen, R.H. and A.M. Johnson (1986) IEEE J. Quantum Electron. **QE-22**, 2154.
Stolen, R.H. and C. Lin (1978) Phys. Rev. A **17**, 1448.
Stolen, R.H., E.P. Ippen, and A.R. Tynes (1972) Appl. Phys. Lett. **20**, 62.
Stolen, R.H., V. Ramaswamy, P. Kaiser, and W. Pleibel (1978) Appl. Phys. Lett. **33**, 699.
Stolen, R.H., C. Lee, and R.K. Jain (1984a) J. Opt. Soc. Am. B **1**, 652.
Stolen, R.H., W. Pleibel, and J.R. Simpson (1984b) IEEE J. Lightwave Technol. **LT-2**, 639.
Stolen, R.H., C.V. Shank, and W.J. Tomlinson (1984c) Procedure for calculating optical pulse compression from fiber-grating combinations. In *Ultrafast Phenomena IV*, D.H. Auston and K.B. Eisenthal, eds., p. 46. Springer-Verlag, Berlin.
Stolz, B., U. Osterberg, A.S.L. Gomes, W. Sibbett, and J.R. Taylor (1986) IEEE J. Lightwave Technol. (1986) **LT-4**, 55.
Strickland, D. and G. Mourou (1985) Opt. Commun. **56**, 219.
Suzuki, T. and T. Fukumoto (1976) Electron. Commun. Jpn. **59-C(3)**, 117.
Tai, K. and A. Tomita (1986a) Appl. Phys. Lett. **48**, 309.
Tai, K. and A. Tomita (1986b) Appl. Phys. Lett. **48**, 1033.
Thurston, R.N., J.P. Heritage, A.M. Weiner, and W.J. Tomlinson (1986) IEEE J. Quantum Electron. **QE-22**, 682.
Tomlinson, W.J. and W.H. Knox (1987) J. Opt. Soc. Am. B **4**, 1404.
Tomlinson, W.J., R.H. Stolen, and C.V. Shank (1984) J. Opt. Soc. Am. B **1**, 139.
Tomlinson, W.J., R.H. Stolen, and A.M. Johnson (1985) Opt. Lett. **10**, 457.
Treacy, E.B. (1968) Phys. Lett. **28A**, 34.
Treacy, E.B. (1969) IEEE J. Quantum Electron. **QE-5**, 454.
Ueda, Y. and K. Shimoda (1967) Japan. J. Appl. Phys. **6**, 628.
Valk, B., W. Hodel, and H.P. Weber (1984) Opt. Commun. **50**, 63.
Valk, B., W. Hodel, and H.P. Weber (1985) Opt. Commun. **54**, 363.
Weiner, A.M., J.P. Heritage, and R.N. Thurston (1986) Opt. Lett. **11**, 153.

Weiner, A.M., J.P. Heritage, and R.H. Stolen (1988) J. Opt. Soc. Am. B **5**, 364.
Weingarten, K.J., M.J.W. Rodwell, and D.M. Bloom (1988) IEEE J. Quantum Electron. **QE-24**, 198.
Wright, J.V. and B.P. Nelson (1977) Electron. Lett. **13**, 361.
Yang, T.Y., P.P. Ho, A. Katz, R.R. Alfano, and R.A. Ferrante (1985) Appl. Opt. **24**, 2021.
Zel'dovich, B.Y. and I.I. Sobel'man (1971) JETP Lett. **13**, 129.
Zhao, W. and E. Bourkoff (1988) IEEE J. Quantum Electron. **QE-24**, 365.
Zysset, B., W. Hodel, P. Beaud, and H.P. Weber (1986) Opt. Lett. **11**, 156.

Robert R. Alfano
Editor

The Supercontinuum Laser Source

With 250 Illustrations

Springer-Verlag
New York Berlin Heidelberg
London Paris Tokyo

ROBERT R. ALFANO
Distinguished Professor of Science and Engineering
Institute for Ultrafast Spectroscopy and Lasers
Physics and Electrical Engineering Departments
The City College of New York
New York, NY 10031, USA

Library of Congress Cataloging-in-Publication Data
The Supercontinuum laser source / Robert R. Alfano, editor.
p. cm.
Includes bibliographies and index.
Contents: Theory of self-phase modulation and spectral broadening / Y.R. Shen, Guo-Zhen Yang — Supercontinuum generation in condensed matter / Q.Z. Wang, P.P. Ho, R.R. Alfano — Ultrashort pulse propagation in nonlinear dispersive fibers / Govind P. Agrawal — Cross-phase modulation: a new technique to control the spectral, temporal, and spatial properties of ultrashort pulses / P.L. Baldeck, P.P. Ho, R.R. Alfano — Simple models of self-phase and induced-phase modulation / Jamal T. Manassah — Self steepening of optical pulses / B.R. Suydam — Self-focusing and continuum generation in gases / Paul B. Corkum and Claude Rolland — The utilization of UV and IR supercontinua in gas-phase subpicosecond kinetic spectroscopy / J.H. Glownia, J. Misewich, P.P. Sorokin — Applications of supercontinuum / R. Dorsinville, P.P. Ho, J. Manassah, R.R. Alfano — Pulse compression and femtosecond continuum / C. Shank and A. Johnson.
1. Laser pulses, Ultrashort. 2. Nonlinear optics. I. Alfano, R.R.
QC689.5.L37S87 1989
621.36'6—dc19
88-8481

Printed on acid-free paper

Cover shows supercontinuum generation of intensity vs. wavelength for 1 mm of carbon tetrachloride liquid excited by a 120-fs, 625-nm laser pulse. Photo by R. Alfano, A. Katz, and P. Ho.

Typeset by Asco Trade Typesetting Ltd., Hong Kong.
Printed and bound by Edwards Brothers, Inc., Ann Arbor, Michigan.
Printed in the United States of America.

9 8 7 6 5 4 3 2 1

ISBN 0-387-96946-2 Springer-Verlag New York Berlin Heidelberg
ISBN 3-540-96946-2 Springer-Verlag Berlin Heidelberg

To my father, Alfonso L. Alfano
and my father-in-law, Samuel J. Resnick
whose advice I deeply miss.